Artificial Intelligence for Engineering Design, Analysis and Manufacturing

www.cambridge.org/aie

Research Article

Cite this article: Naeini MS, Machado M and Dutkiewicz M (2025). Convolutional autoencoder for on-demand parametric inverse design of local resonator geometry in wind turbine metastructure targeting vibration control. Artificial Intelligence for Engineering Design, Analysis and Manufacturing, 39, e24,

https://doi.org/10.1017/S0890060425100139

Received: 24 February 2025 Revised: 28 July 2025 Accepted: 11 August 2025

Keywords

deep learning; latent space exploration; supervised autoencoder; parameter-based inverse design; sensitivity optimization method

Corresponding author:

Marcela Machado; Email: marcelam@unb.br

© The Author(s), 2025. Published by Cambridge University Press. This is an Open Access article, distributed under the terms of the Creative Commons Attribution licence (http://creativecommons.org/licenses/by/4.0), which permits unrestricted re-use, distribution and reproduction, provided the original article is properly cited.



Convolutional autoencoder for on-demand parametric inverse design of local resonator geometry in wind turbine metastructure targeting vibration control

Mohammadreza Sahaf Naeini¹, Marcela Machado^{1,2} o and Maciej Dutkiewicz¹

¹Faculty of Civil, Environmental Engineering and Architecture, Bydgoszcz University of Science and Technology, Bydgoszcz, Poland and ²Department of Mechanical Engineering, University of Brasilia, Brasilia, Brazil

Abstract

Vibration control in structures is essential to mitigate undesired dynamic responses, thereby enhancing stability, safety, and performance under varying loading conditions. Mechanical metamaterials have emerged as effective solutions, enabling tailored dynamic properties for vibration attenuation. This study introduces a convolutional autoencoder framework for the inverse design of local resonators embedded in mechanical metamaterials. The model learns from the dynamic behaviour of primary structures coupled with ideal absorbers to predict the geometric parameters of resonators that achieve desired vibration control performance. Unlike conventional approaches requiring full numerical models, the proposed method operates as a data-driven tool, where the target frequency to be mitigated is provided as input, and the model directly outputs the resonator geometry. A large dataset, generated through physics-informed simulations of ideal absorber dynamics, supports training while incorporating both spectral and geometric variability. Within the architecture, the encoder maps input receptance spectra to resonator geometries, while the decoder reconstructs the target receptance response, ensuring dynamic consistency. Once trained, the framework predicts resonator configurations that satisfy predefined frequency targets with high accuracy, enabling efficient design of passive controllers of the syntonized mass type. This study specifically demonstrates the application of the methodology to resonators embedded in wind turbine metastructures, a critical context for mitigating structural vibrations and improving operational efficiency. Results confirm strong agreement between predicted and target responses, underscoring the potential of deep learning techniques to support on-demand inverse design of mechanical metamaterials for smart vibration control in wind energy and related engineering applications.

Introduction

Wind turbines face various challenges, including vibrations caused by environmental phenomena that affect their performance, reduce efficiency, and sometimes lead to significant problems that can cause system malfunctions (Machado and Dutkiewicz, 2024). Various approaches can be employed to overcome this problem. Conventional methods include the use of dampers, absorbers, and structural reinforcements to control undesired vibrations. However, these approaches can be inefficient due to their increased weight and complexity. On the other hand, metamaterials offer an innovative approach by utilizing engineered structures rather than relying solely on material properties. Metamaterials have the potential to control wave propagation through specially designed structures that can redirect absorbed energy or even dampen energy from vibrations. They enable the integration of passive vibration control in various fields, thereby potentially enhancing both operational performance and lifespan. Metamaterials designed with dynamic resonators can improve vibration mitigation in the structure and have been proven to be efficient in controlling the vibration of wind turbines (Machado et al., 2024).

Mechanical metamaterials exhibit unique mechanical properties and advantages over conventional materials, offering benefits such as negative stiffness and mass density optimized for specific frequency ranges to enhance vibration isolation (Hussein et al., 2014; Dalela et al., 2022; Valipour et al., 2022; Sinha and Mukhopadhyay, 2023). These metamaterials typically form periodic structures with resonators, mass, geometry, and other characteristics, achieving superior vibration suppression in the bandgap regions compared with traditional absorbers (Brennan, 2006). Based on dynamic vibration absorber concepts, local resonators have been widely explored. Combining various materials and physics in resonators enhances metamaterial properties, such as electro-mechanical systems (Machado et al., 2019; de Moura et al., 2024), and fluid—solid combinations (Zhang et al., 2018; Wu and Li, 2021; Dutkiewicz and Machado, 2019a,



2019b, 2019c). The design process of those metamaterials begins with investigating mechanisms at the physical level, followed by designing dynamic features to achieve the desired tuned frequencies for applications such as vibration control. This involves proposing periodic patterns and determining the physical and geometrical properties for global-level fabrication, given the significant challenges posed by macro-structure complexity (Jiao and Alavi, 2022). Henceforth, designing the forward dynamic features of the metamaterial resonators for vibration control applications can be effortless. Therefore, the physical design associated with the geometry and mechanical properties of those resonators, following their dynamic characteristics, can be complex. In Machado et al. (2024), the authors proposed using mechanical metamaterials with dynamic absorbers distributed along the length of the turbine in complex systems such as wind turbines. These absorbers are designed to dynamically match the turbine's operational frequencies, enhancing vibration control. However, traditional methods for designing these resonators, which combine numerical simulations and empirical tuning, are time-consuming, lack generalization capabilities, and are computationally intensive.

Researchers have employed computational techniques, such as topology optimization, to design and fabricate complex metamaterial structures. Conventional optimization techniques, such as evolutionary algorithms (Colherinhas et al., 2022; Reis and Karathanasopoulos, 2022; Cerniauskas and Alam, 2023), topology optimization (Han et al., 2023), and the particle swarm method (Li et al., 2024), are employed to address the computational complexity associated with metamaterial design problems. Recent studies have shown the ability of machine learning (ML) approaches to solve inverse design problems. In this respect, ML models can be trained to recognize the patterns between input parameters and the desired output, enabling the rapid prediction of designs that meet specific specifications. The development of artificial intelligence techniques, including ML, deep learning (DL), and generative methods, has recently addressed design engineering problems that can be complex, costly, and time-consuming to solve using conventional approaches. The inverse design approach systematically produces a design of metamaterials for specific mechanical objectives, such as negative stiffness, geometry, high damping, or targeted frequency response (Cerniauskas et al., 2024).

ML has received remarkable attention in the last few decades. These methods can be used in monitoring (Sousa et al., 2023; Coelho et al., 2024; Soomro et al., 2024) and understanding the patterns between the parameters and the target. In Otaru (2023), the author employed artificial neural networks to predict the sound absorption properties of cellular materials with an accuracy of over 95%, showing the power of ML to analyze the complex relationship between signals and parameters. Recent advancements in ML methods focused on both forward prediction and inverse design. Among these techniques, DL has become a powerful tool in designing and optimizing metamaterials, offering significant advantages over traditional methodologies. In this approach, neural networks are exploited to predict the properties of metamaterials, allowing higher efficiency and accuracy. DL-based inverse design methods leverage the power of deep neural networks (DNNs) to address the limitations of traditional approaches. DNNs can learn sophisticated relationships between input and output, significantly enhancing forward prediction and inverse design by learning physical processes and generating functional designs. This results in reduced computational time and a better design process. For example, DL-based models can design and optimize metamaterials that exhibit different responses, eliminating time-consuming numerical

simulations (Ma et al., 2018; Ashalley et al., 2020; Hou et al., 2020; Hou et al., 2021; Zhang et al., 2021). Additionally, these models enable inverse design based on the desired performance criteria. For instance, researchers have exploited DL methods to create customized metamaterials, simplifying the design process and allowing automatic inverse design across different metasurfaces (Chen et al., 2019; Hou et al., 2020). In Inampudi and Mosallaei (2018), the authors used a neural network to predict the contact angle and contact diameter of nanowires with material parameters. They show the effectiveness of ML techniques in accurately predicting physical properties. The inverse design based on neural networks for material and optical design has been proposed in Cerniauskas et al. (2024) and Jin et al. (2022). In Jin et al. (2022) and He et al. (2023), researchers conducted a literature review on new developments in the inverse design of metamaterials, highlighting advancements in this field, including controlling vibration (Chen et al., 2022; Dedoncker et al., 2023; Li et al., 2024), phononic and acoustic metamaterials and manipulation of waves (Goh and Kallivokas, 2019; So et al., 2020; Wu et al., 2021; He et al., 2022; Jin et al., 2022; Muhammad and Kennedy, 2022), and acoustic absorption (Mahesh et al., 2021; Gao et al., 2022), where DL algorithms are used for managing the vibrational energy.

DL frameworks are particularly effective in providing rapid and accurate predictions for the design of phononic crystals and elastic metamaterials, thereby overcoming the limitations of traditional design methodologies (Liu and Yu, 2023). These models deliver high prediction accuracy with low computational costs, making them ideal for tackling complex inverse design challenges (Chen et al., 2019; Raju et al., 2022). Peurifoy et al. (2018) proposed a fully connected neural network to approximate the light-scattering simulations in a supervised manner. Their approach significantly reduced the computational cost of inverse-designing nanophotonics compared to traditional methods. Yabin et al. (2022) designed a network based on fully connected layers (FCLs) to inverse design an Archimedean spiral metastructure, aiming to find the radius and width of the spiral arm of the metastructure by feeding the center frequency and the width of the bandgap to the model. They successfully validated their model using results obtained from Finite Element Method (FEM) and experiments, demonstrating the power of DL in the inverse design of metastructures. Furthermore, generative adversarial networks and capsule networks facilitate the generation of samples that can be used to satisfy specific criteria by understanding the underlying patterns between the features and targets (Guo et al., 2023).

On the other hand, unsupervised learning methods manage data without labels, so the network tries to extract essential patterns from the data without requiring labeled outputs. Among DL architectures, one of the most commonly used architectures in inverse design is the autoencoder (AE). The AE is an unsupervised DL network primarily used for image processing, anomaly detection, and dimensionality reduction. Harper et al. (2020) implemented a pseudo-AE to predict the metasurface's design from desired reflection and transmission spectra. With their proposed methodology, they improved the efficiency and performance of the metasurface. Soete et al. 2024 used an AE to extract topological features from phononic crystals. Then they used these features as input to train a fully connected dense layer for mapping between topological features and band gaps. Their method enabled the inverse design of phononic crystals to achieve the expected band gaps. Recent advancements in mechanics-informed AEs have demonstrated that embedding physical constraints into the latent space can also enhance performance in structural health monitoring (Soete

et al., 2024). In addition, generative neural networks and reinforcement learning models have been applied to the inverse design of acoustic metamaterials (Wang et al., 2020), mechanical metamaterials with targeted nonlinear deformation (Brown et al., 2023), and auxetic metamaterials (Zhang et al., 2023), showcasing their potential to create structures with customized mechanical properties. Variational AEs further enhance this capability by mapping complex microstructures into a low-dimensional latent space. A design simplification for intricate microstructures and multiscale metamaterial systems was investigated in Amirkulova et al. (2022), as well as for ultra-broadband acoustic metamaterials by Cho et al. (2024).

Although FCLs have proven useful in AEs, subsequent development has demonstrated the incorporation of convolutional neural networks (CNNs) and recurrent layers within AE structures due to the potential of these architectures in extracting spatial and temporal characteristics. Shi et al. (2020) proposed AMID, a twodimensional (2D) CNN-based AE for extracting dimensional features from grayscale representations of electromagnetic properties. These features were then used with an optimized Support Vector Machine (SVM) to design metasurfaces inversely based on specified electromagnetic characteristics. Zhang et al. (2024) employed a pretrained ResNet18-based CNN backbone as a feature extractor to learn fault characteristics from vibrational signals and proposed a framework for machinery fault diagnosis. Moreover, Ren et al. (2024) proposed a novel intelligent fault diagnosis method for bearings using a multihead self-attention CNN. Further, Donda et al. (2021) proposed a DL approach to derive absorption spectrum responses of metasurface absorbers using a 2D CNN architecture. Not only did they significantly reduce the computational time compared to FEM, but they also, by exploiting their network, modeled an ultra-thin metasurface with absorption at extremely low frequencies. Mahesh et al. (2021) and (2024) utilized one-dimensional (1D) CNNs to design resonators with an inverse approach, focusing on the absorption coefficient. They demonstrated the effectiveness of convolutional layers in capturing spatial patterns in the signals. The power of CNNs is not limited to signals or images, and they can be used to extract features from all kinds of inputs; for instance, Li et al. (2024) proposed a character-level TextCNN model to extract features directly from the sequence of characters in raw data frames, enabling the automatic construction of information models needed for industrial system integration. Furthermore, long short-term memory (LSTM) and bidirectional LSTMs are highly effective for extracting temporal relations within the data. Pillai et al. (2021) used LSTM-based neural networks to model the sequential nature of spectral responses in metamaterials. They treated the inverse design problem as a sequence-to-sequence learning task. This approach enabled them to predict structural parameters from desired electromagnetic properties accurately. They leveraged the power of LSTM layers to find dependencies within spectral data. Moreover, Jiang et al. (2023) demonstrated the ability of LSTM-based models to address complex industrial problems; their model successfully captured time-dependent relationships between the robot's motion history and its power usage to predict and optimize energy consumption. In a subsequent study, Jiang et al. (2025) incorporated 1D-CNN layers to denoise and extract features from signals before feeding them to LSTM layers, thereby improving the prediction accuracy in their hybrid-driven paradigm. These models can optimize different systems, such as damping systems, actuators, or material compositions, to improve vibration control performance while balancing computational complexity with real-time constraints.

There are two conventional methods commonly used by researchers for inverse design: (1) the binary pixel image-based approach, which predicts the pixels in an image that correspond to the shape of the structure for the desired spectrum, and (2) the parameter-based approach, which predicts the geometric parameters corresponding to the desired spectrum. Each of these methods has its advantages and limitations. The binary pixel image-based approach is suitable for designing complex structures and offers a broad design space. However, the computational time of this approach is very high (Cho et al., 2024). On the other hand, the parameter-based approach is more computationally efficient. However, its main limitation is its low design flexibility, as the structure is defined by a limited number of parameters that make it difficult for models to relate the parameters to the spectrum. Achieving on-demand performance with traditional approaches is a significant challenge. Inverse designing metamaterials by exploiting AE can be applied in different applications. However, this article focuses explicitly on designing mechanical metamaterials tailored to control vibration responses. To our knowledge, no previous work has used an AE-based CNN model to design a local resonator of a mechanical metastructure aiming vibration control.

At the industrial level, dynamic passive control devices, such as dynamic absorbers, must adopt manufacturable geometries while meeting specific performance criteria. Transitioning from ideal dynamic models to physical implementations poses challenges, particularly in ensuring that device parameters align with desired dynamic properties for effective control and system reliability. Although classical closed-form expressions can estimate the ideal operating frequency and dynamic response, they do not directly yield viable geometries, as the physical design depends on complex interactions between material and geometry. Since the primary structure's dynamic behavior dictates the configuration of passive controllers, determining their geometric characteristics becomes an inherently complex optimization problem. This study proposes a parametric inverse design model using a CNN-AE to predict the geometric attributes of dynamic resonators embedded in metastructures, guided by the desired dynamic response of the host structure to be mitigated. The main contributions of the work are: (i) the development of a CNN-AE architecture tailored for on-demand inverse design of passive controller geometries for vibration control, and (ii) the incorporation of dynamic response data as input in the DL model to establish a direct mapping between the desired dynamic characteristics and the physical geometry of ideal controllers. The model is trained, validated, and tested in a case study involving a wind turbine using a database generated from a numerical model, including responses from various dynamic absorbers across a target frequency range. The proposed DL approach offers a scalable and fast alternative to traditional analytical or iterative optimization methods, enabling non-iterative prediction of feasible, manufacturable geometries. The CNN-AE architecture, with its layered design, mitigates the limitations of parameter-based methods and accelerates the design process. The model successfully predicted the geometry of a local resonator embedded in a wind turbine metastructure designed for vibration attenuation, meeting the required dynamic performance. Validation showed strong agreement between the resonance frequency of the predicted geometry and that of the target spectrum, demonstrating the model's reliability and highlighting the potential of DL for tailored passive vibration control solutions.

Forward design of the metamaterial wind turbine resonator

A 2D metamaterial turbine spectral model was proposed and validated in Machado et al. (2024) and Machado and Dutkiewicz (2025). The spectral element method was employed to model the wind turbine metastructure due to its modeling reduction capabilities compared to the Finite Element Method, efficiency in computational effort, high accuracy in dynamic solutions, and its ability to express solutions in the frequency domain. The monopile turbine metastructure is constructed with a tapered-shaped tower, where the cross-sectional area of each beam element gradually reduces from the base to the top. The first three elements from the base have a similar cross-section, each with a diameter of 6 m. Their diameters and thicknesses gradually decrease toward the top of the tower, with the final element (number 13) representing the smallest diameter. Each element is attached to a dynamic resonator, and the top element is also coupled to the lumped mass that represents the nacelle and blades. The weak form of the beam attached to a resonator element equation of motion is evaluated under the weighted-integral statement in an arbitrary variation of the displacement ν . Assume there are \overline{n} resonators attached to the beam at locations v_{z_r} , with masses m_r , stiffness k_r , natural frequencies $\omega_r^2 = k_r/m_r$, and relative displacements u_r , it is defined in the frequency domain as (Machado and

$$\int_{t_1}^{t_2} \left[\int_0^L EIv'' \delta v'' - \omega^2 \int_0^L \rho A v \delta v - \sum_{r=1}^{\overline{n}} m_r \omega_r^2 u_r \delta(z - z_r) dz - \int_0^L F \delta(z - z_f) \delta v dz \right] dt = 0$$
 (1a)

$$\int_{t_1}^{t_2} \left[\sum_{r=1}^{\overline{n}} m_r \frac{\mathrm{d}^2 u_r}{\mathrm{d}t^2} + k_r (u_r - v_{z_r}) \right] dt = 0$$
 (1b)

where ' denotes space derivation, δ virtual displacement, EI the flexural rigidity, ρA mass, and F the external force. The unit cell of the system for dynamic modeling considers one element of the mesh. The wind turbine modeling consists of 14 elements in the global matrix assembly, similar to the finite element method. For the detailed formulation and modeling, we suggest the recent development present in Machado et al. (2024) and Machado and Dutkiewicz (2025). The turbine metastructure numerical model is employed in the final inverse design stage to test the control efficiency.

Dynamic modeling of the ideal locally resonator

Tuned mass dampers, which serve as dynamic vibration absorbers, are commonly implemented as a passive technique to reduce vibrations in wind turbines due to their simplicity and efficiency. These systems typically simultaneously address up to two resonant frequencies, exploring their placement and overall characteristics within the structure. They operate passively, relying on their inherent damping and stiffness properties to dissipate energy without requiring external power sources. Activation occurs in response to vibrations from the primary structure to which they are attached, ensuring cost-effectiveness and minimal maintenance requirements. The initial dynamic design of such a passive dynamic control resonator typically follows an analytical solution.

The resonant frequencies of the NREL 5 MW offshore wind turbine exhibit clear separations from one another, with the design of the control systems and their specific characteristics outlined individually. In contrast, the metastructure arrangements are composed of an array of resonators as presented in Figure 1. In the specified subdomain of the turbine metastructure consisting of N-resonators displaced periodically, where $\Delta L_j = \int_{L_j} dL$ represents the length of subdomain $a = L_j$. Furthermore, the spring coefficient of each cantilever resonator is assumed to be uniform. The mass of each resonator is determined by $m_r = \epsilon m \Delta L$ (Sugino and Erturk, 2016), the mass ratio referred to as $\epsilon = \sum_{p=1}^N m_r / \int_L m(x) dL$, for m(x) represents the mass density at a specific point within the domain. The equation of motion that describes the ideal resonators is given as follows

$$m_r \ddot{u}_r(t) + k_r u_r(t) + m_r \ddot{v}_{z_r}(x, p, t) = 0$$
 $r = 1, 2, ..., N$ (2)

where $v_{z_r}(x,p,t)$ represents the displacement of a point with a position vector r to the turbine tower, which is considered the primary system. The variables k_r , m_r , and $u_r(t)$ denote the stiffness, mass, and displacement of the p^{th} resonator relative to the primary structure, respectively. The relative displacement, represented by $u_r = (u_r - v_{z_r}(x_p))$, indicates the displacement of each r^{th} resonator concerning the relative displacement of the primary structure, denoted by $(v_{z_r}(x_p))$. The natural frequency and displacement response of an ideal resonator are defined simply by the mass and stiffness parameters represented by

$$\omega_r = \sqrt{k_r/m_r}$$
 $r = 1, 2, ..., N$ and $\boldsymbol{u}_r(\omega) = \frac{f}{k_r - \omega^2 m_r}$ (3)

Hysteretic damping is assumed for the resonator spring, described by a complex stiffness expressed as $k_r = \overline{k}_r (1+i\zeta)$, which is often associated with dry friction in materials. In a real application, the controller's tuned frequency should match the primary system's desired frequency to be attenuated. For the parametric design of the resonator, both geometry and material are required. The position of the lumped mass in each absorber is calculated following Dunkerley's semi-empirical formulation, which gives a lower band approximation (Jeffcott, 1918) to satisfy the tuning frequency condition

$$\frac{1}{\omega_{ab_{j}}^{2}} \simeq \frac{1}{\omega_{beam}^{2}} + \frac{1}{\omega_{m_{0}}^{2}}, \quad j = \{1, 2, 3\}$$
 (4)

where

$$\omega_{beam} = 3.5160 \sqrt{\frac{E_{beam}I_{beam}}{m_{beam}L_{beam}^3}}, \qquad \omega_{m_0} = \sqrt{\frac{6E_{beam}I_{beam}}{m_{ab_i}l_{ab_i}^2(3L_{beam} - l_{ab_i})}}$$

Hence, the tuning frequency of the absorber depends on an optimal parameter: the position of the mass along the absorber beam, denoted by l_{ab_i} , as well as on the geometry of the beam and the attached mass. This tuning process involves optimization techniques and requires significant computational and methodological effort. The dynamic response of the resonator exhibits a multivariable dependence on both geometric and material parameters. In this work, the material properties are predefined, and the geometry is obtained through inverse design using the CNN-AE model. The dynamic response of the resonator, in this case, depends on the parameter vector $\boldsymbol{\theta} = [b_r, h_r, l_r]$ and is characterized by

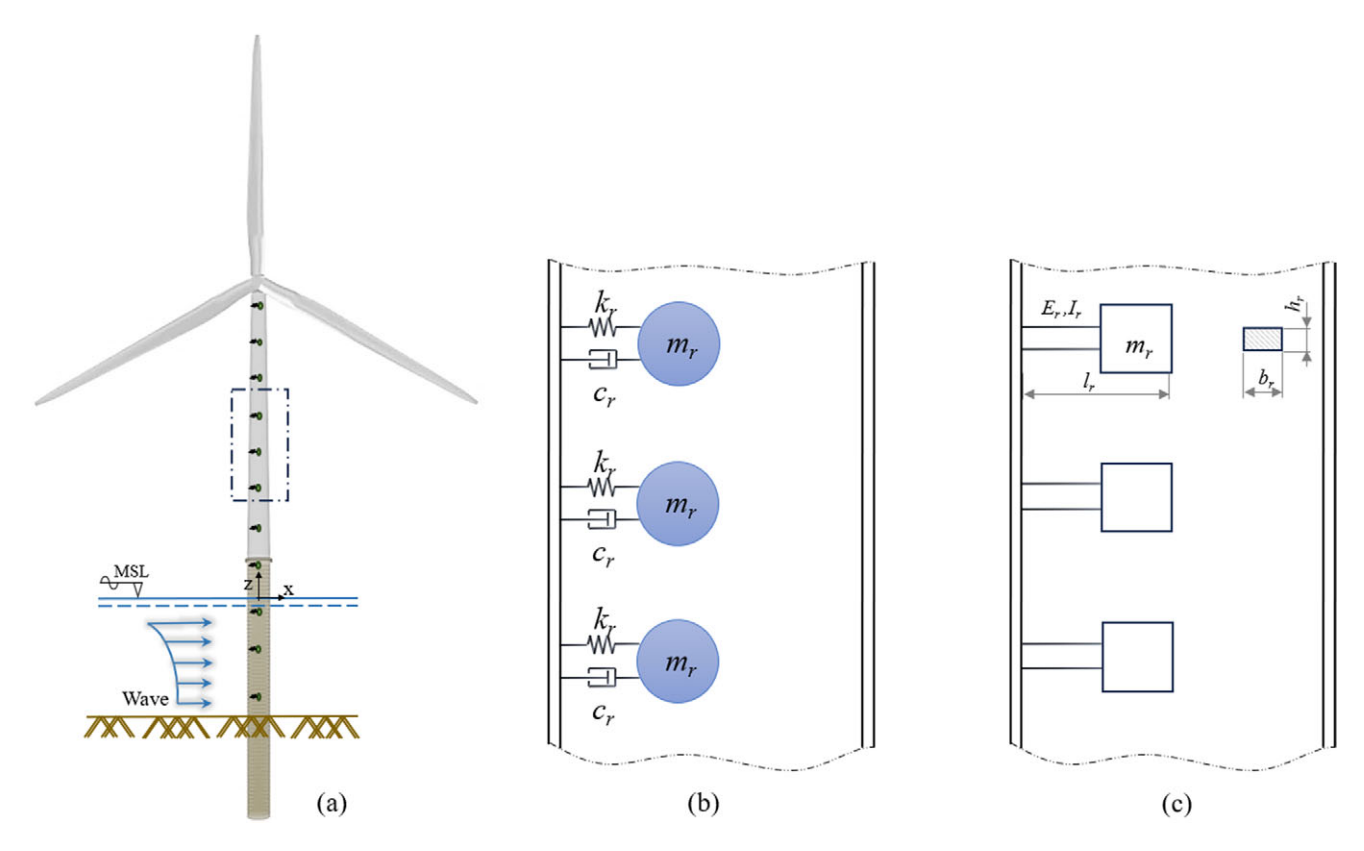


Figure 1. Schematic representation of the metamaterial 5 MW NREL offshore wind turbine (a), zoom details of ideal dynamic resonators used in the forward design (b), and physical resonators obtained by the inverse design (c).

$$\boldsymbol{u}_{r}(\omega,\theta) = \left[\frac{3E_{r} \frac{b_{r} h_{r}^{3}}{12}}{l_{r}} - \omega^{2} \rho_{r} b_{m_{0}}(\theta) h_{m_{0}}(\theta) l_{m_{0}}(\theta) \right]^{-1} f(\omega), \quad (5)$$

where the subscripts r and m_0 refer to the beam and the combined beam and lumped mass components, respectively. It is important to note that the total mass is influenced by both the lumped mass and the geometric mass of the beam. Since no closed-form solution exists for this system, an optimization method is required to determine the optimal design parameters.

Evaluation of the local resonant metastructure design

Metamaterials are artificial composite materials composed of periodically arranged unit cells containing internal substructures, such as resonators or patterns, designed to manipulate properties not found in natural materials. This periodic tessellation enables consistent dynamic behavior that can be described using homogenized effective properties, such as negative mass or stiffness (Liu and Hussein, 2012). For homogenization to hold, the unit cell must be much smaller than the wavelength, leading to a subwavelength condition $a/\lambda \ll 1$, and the overall structure should be at least an order of magnitude larger than the unit cell, ensuring sufficient scale separation.

In finite structures, such as wind turbine towers, where flexural wave propagation dominates, the resonators must be geometrically tuned to the target frequency and positioned at subwavelength intervals. These resonators, initially idealized as mass-spring systems, are associated with a specific vibration mode (Dedoncker et al., 2023). When applied in periodic or quasi-periodic arrays, they can induce locally resonant bandgaps or attenuation bands.

While bandgap formation is often analyzed assuming infinite periodicity and traveling waves, the response of finite structures is more closely tied to modal interactions (Cleante et al., 2022). This feature enables applications such as low-frequency vibration attenuation and wave filtering analysis, even when the wavelength is larger than the unit cell size (El-Borgi and Fernandes, 2020). In wind turbine metastructures, as in other local resonant metamaterial types, embedding resonators designed for local resonance allows the formation of effective attenuation bands, enhancing vibration control within the subwavelength regime (Liu and Hussein, 2012). To demonstrate analytical insight, the concept of infinite absorbers is applied and extended to finite structures, following the approach presented in Sugino and Erturk (2016) Machado and Dutkiewicz (2024). In this context, resonators are periodically distributed along the host structure with a unit cell length constant of $a = L/10 \ll \lambda$, deliberately chosen to ensure subwavelength spacing relative to the flexural wavelength λ . This condition is essential for enabling effective metamaterial behavior through local resonances. The phase velocity of flexural waves in beam-like structures is frequency-dependent (dispersive), and the wavelength and unit cell length are given by

$$c = \frac{\omega}{k_{\nu}} = \left(\frac{EI}{\rho A}\right)^{1/4} \omega^{1/2}, \quad \lambda = \frac{2\pi}{k_{\nu}} = \frac{c}{f},$$

$$a \begin{cases} \leq \frac{\lambda}{5} & \text{typical metamaterial limit} \\ \leq \frac{\lambda}{10} & \text{safe homogenization bound} \end{cases}$$
(6)

where *E* is the Young's modulus, *I* is the second moment of area, ρ is the material density, *A* is the cross-sectional area, $\omega = 2\pi f$ is the

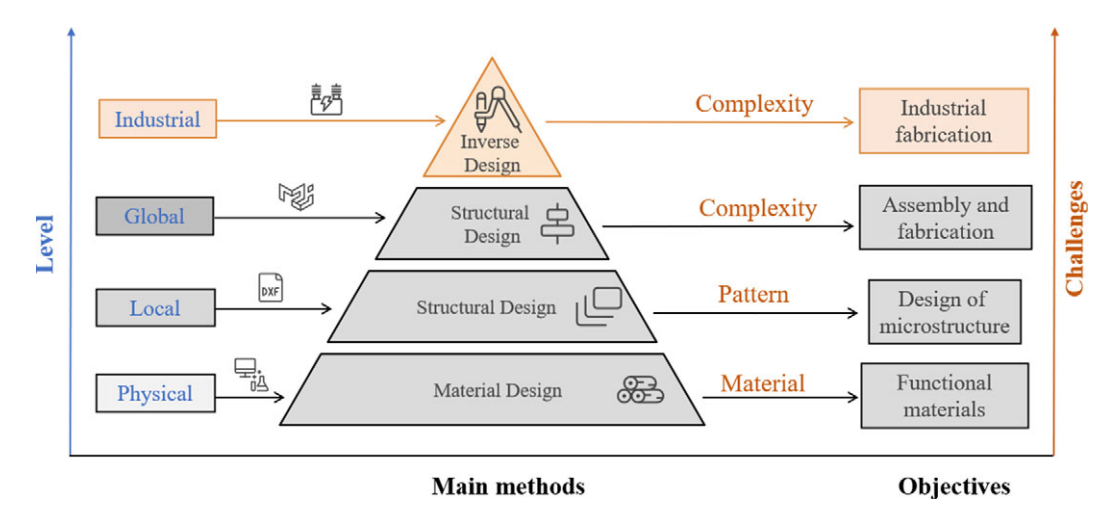


Figure 2. Four levels designing chain of metastructures associated with methods, challenges, and objectives (adapted from Jiao and Alavi, 2022]).

angular frequency, and k_v is the wavenumber. The standard homogenization criteria follow the typical metamaterial limit, as defined in Sridhar et al. (2016) and Ariza et al. (2024).

Hence, to verify whether the local resonator metastructure operates in the subwavelength regime, a necessary condition for achieving metamaterial-like behavior in vibration attenuation is that it is sufficient to ensure that the unit cell length a is significantly smaller than the λ . This evaluation is conducted using the geometric and material parameters of the NREL 5-MW reference wind turbine tower (Jonkman et al., 2009), with a focus on the lowfrequency range around 0.3 Hz, where flexural behavior governs the dynamic response. The flexural stiffness of the wind turbine is $EI = 2.94 \times 10^{12}$ Nm², and the inertial term is $\rho A \approx 3699.5$ kg/m. Substituting into Eq. (6), the flexural wavelength at f = 0.3Hz is $\lambda \approx 816$ m. For the tower height around 100 m, results in a unit cell spacing $a \approx 10$, yielding $\frac{a}{\lambda} \approx 0.013 \ll 1$, confirming operation in the subwavelength regime. Therefore, the tower-resonator configuration satisfies subwavelength criteria, enabling resonance-based wave attenuation mechanisms characteristic of metamaterials. However, since the structure contains only a few discrete resonators and does not exhibit wide-range periodicity, we adopt the terminology of local resonant metastructure rather than claiming a homogenized metamaterial in the strict sense.

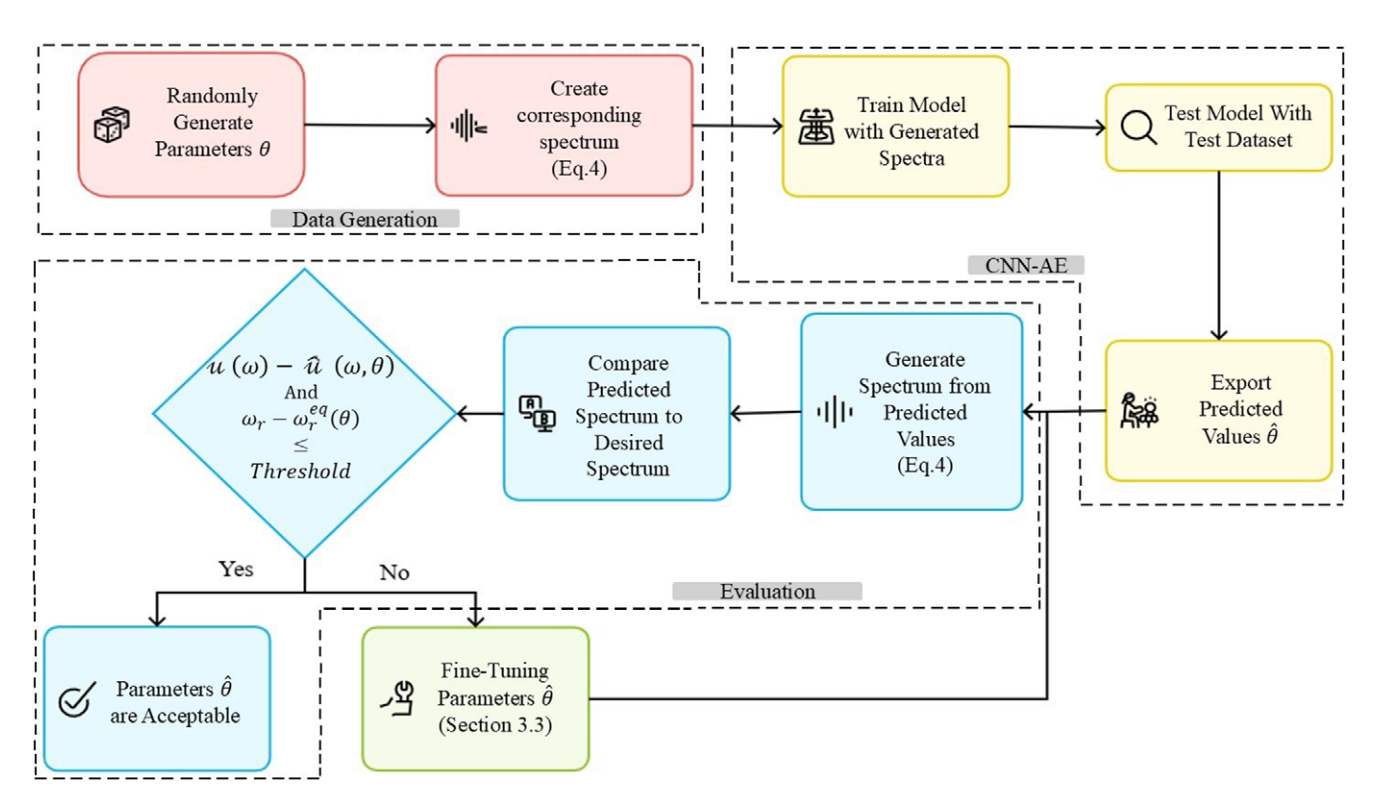
Inverse design using a convolutional AE

At the industrial level, dynamic passive control, as dynamic absorbers, must adopt manufacturable geometries and meet specific design criteria. Transitioning from ideal dynamic models to physical implementations introduces challenges, particularly in ensuring that the device's parameters align with the required dynamic properties for effective control and system reliability. While the ideal operating frequency and dynamic response of a resonator can be estimated using classical closed-form expressions (Eq. 3), these simplified mass-spring models do not directly yield viable geometries, as the physical design depends on material and geometry interactions. Addressing these constraints typically requires an iterative optimization process. The proposed DL strategy offers a scalable alternative to traditional analytical or optimization methods by enabling a fast, non-iterative prediction of suitable geometries, integrating a data-driven process. This approach

addresses dynamic requirements and manufacturable designs, facilitating the practical deployment of passive controllers.

Mechanical metamaterial design spans four hierarchical levels as physical, local, global, and industrial, each increasing in complexity and methodological demands (Jiao and Alavi, 2022). As shown in Figure 2, the physical level focuses on intrinsic material properties, the local level on microstructural design, and the global level on structural-scale fabrication. The industrial level addresses real-world deployment, requiring reliable and cost-effective solutions that link micro- and macroscale performance. Here, inverse design becomes essential for aligning structural behavior with performance goals. This study proposes an inverse design strategy for dynamic absorbers in industrial applications, enabling the rapid and on-demand development of passive controllers based on the host structure's dynamics. The method employs a CNN-AE with model updating to improve accuracy and ensure manufacturable output.

The inverse model was developed as a data-driven framework to guide practical applications, where the target control frequency is provided as input, eliminating the need for a numerical model. The interaction between the primary structure and the resonator is assessed after the inverse design stage. If fine-tuning is necessary, rapid recalculations of the resonator geometry are enabled through an embedded sensitivity-based model. The proposed model predicts the geometric parameters of the local resonator embedded in the turbine metastructure, having as prior information the frequency spectrum of an ideal resonator. Integrating the target spectral signature into the design workflow effectively translates system-level dynamics into physical configurations. The model outputs the resonator geometry while considering a predefined mass ratio, resonator location, material, and the dynamic characteristics of the host structure. In the presented application, the cantilever resonator's height, width, and length are the design variables. Although limited to three parameters, the inverse design problem remains challenging due to its coupling with the controller mass. While topology optimization is beyond the present scope, this approach provides a foundation for scalable, data-driven inverse design methodologies. The interaction between the controller and the primary system is inherently considered in the numerical model used to evaluate the control performance, which is apart from the DL model.



4:

10:

Figure 3. Workflow of the proposed inverse design model.

Algorithm 1 and Figure 3 present the proposed inverse design workflow, which consists of five main steps. The process begins with input derived from the dynamic resonator's receptance response, enabling efficient and precise parameter prediction. The dataset is generated from analytically computed receptance spectra based on Eq. (5), with the resonator's cantilever geometry defined by randomly sampled parameters (see Section "Data generation"). In the second step, a CNN-AE (Section "CNN-AE model architecture") is trained and tested to map spectral features to geometric parameters within the 0–3 Hz frequency range, which includes the critical resonant frequencies of the target turbine. The trained AE encodes the spectra into a latent space and outputs a cluster of predicted parameters. Steps 1 and 2 are run only once for training the model.

Step 3 performs the on-demand inverse design. It receives a given test or new spectrum input, and the CNN-AE predicts the geometric parameters, in our case, the $\theta = [l_r, b_r, h_r]$, but not limited to these three. Step 4 validates the prediction by comparing the analytically computed receptance response (via Eq. 5) with the target spectrum. If the error is within an acceptable threshold, the prediction is accepted. Otherwise, step 5 applies a sensitivity-based optimization method (Section "Sensitivity optimization method") to fine-tune the parameters until the predicted and reference responses converge. This procedure ensures high accuracy in designing the resonator for optimal dynamic performance.

Algorithm 1 Pseudocode for the dataset generation, training the model, and post-processing the output.

1: **Data generation**: Sampling random variables as described in Section "*Data generation*"

- 2: Receptance response dataset: Calculate $u(\omega, \theta)$ having as input the random parameters
- 3: Data processing: Check for outliers
 - outliers = DetectOutliers(samples)
 - : cleaned data = RemoveOutliers(samples, outliers)
- 6: **Data setting**: Splitting the dataset into Train, Validation, and Test, and normalizing data
- 7: Training the CNN-autoencoder model: CNN-autoencoder-based model proposed in Section "CNN-AE model architecture"
 8: for epoch in range(epochs):
 - for epoch in range (epochs)
- 9: for batch in GetBatches(normalized train data, batch size):

$$\hat{\theta} = \mathscr{B}_{\phi}(\mathbf{u}(\omega))$$

- 11: $\hat{\boldsymbol{u}}(\omega) = \mathcal{D}_{\theta}(\hat{\theta})$
- 12: compute Loss $[\theta, \hat{\theta}, u(\omega), \hat{u}(\omega)]$, given in Eq. (9)
- 13: Update weights
- 14: Receptance generation: Generate spectrum from predicted parameters $(\hat{\theta})$ using Eq. (5)
- 15: Input test dataset to the trained model: Predict the parameters of the tested samples.
- 16: Generate spectrum $\hat{u}(\omega)$ from predicted parameters $(\hat{\theta})$ using Eq. (5)
- 17: Compare desired $u(\omega)$ with generated $\hat{u}(\omega, \hat{\theta})$
- 18: **if** $u(\omega) \hat{u}(\omega, \theta) < 0.001 & \omega_r \omega_r^{eq}(\theta) < 0.02 \text{ Hz}$
 - Predicted parameters are acceptable
- 20: else:

19:

- 21: Parameters fine-tuning by the sensitivity method (Eq. 14)
- 22: Calculate the receptance response with the updated parameters and compare spectra

Data generation

The performance of the DNN model relies on high-quality datasets, where poorly generated samples can lead to an unstable distribution in the design space, negatively affecting the network's performance and reducing accuracy. An imbalanced sample distribution can result in high representation in some areas while leaving others empty, hindering the model's ability to generalize efficiently. Thus, the latin hypercube sampling (LHS) technique (Helton and Davis, 2003) is employed, using the pyDOE library in Python, to sample the dataset. LHS differs from the Monte Carlo technique, which randomly places points within the parameter space. Instead, LHS enables a more accurate parameter space exploration by dividing the sample space into equal fractions. This method divides the cube into rows and columns equal to the total number of desired samples and selects one sample for each row and column to cover the entire range of the design space. This balanced sampling technique improves the quality and accuracy of the model.

The dataset consists of a random realization of the receptance response of the resonator embedded in the metastructure defined by Eq. (5) leading to $\tilde{u}_r(\omega,\tilde{\theta})$. The spectrum for a random assortment of these geometric parameters is generated across a frequency range of 0–3 Hz while keeping all other geometric and material properties constant. The random geometric parameters for data preparation are chosen based on a uniform distribution and are listed in Table 1.

The next preprocessing step is to clean the data and identify outliers. Many models adjust their weights using mean squared error (MSE) as the loss function. However, this metric is highly sensitive to outliers, which can significantly reduce model accuracy. Therefore, outliers must be identified and eliminated. Traditional outlier detection techniques, such as Z-score and interquartile range, which depend on data distribution, are inadequate because the algorithm used to generate samples aims for a uniform distribution over the design space. Instead, an isolation forest algorithm is employed for outlier detection. Further details on its methodology can be found in the original article (Liu et al., 2008). Using this method, ~2,000 outliers were identified and removed from the database to ensure data quality for training models, resulting in 198,000 samples for model training. These samples are then split into a training set (80%), a validation set (10%), and a test set (10%). They are then normalized using Min-Max Scaling to a range between zero and unity.

AE architecture of the inverse design algorithm

The on-demand inverse design of a mechanical resonator presents a significant challenge, due to the complex and nonlinear relationships between a resonator's geometry and its dynamic response. The receptance spectrum is a high-dimensional data vector that may include redundant information. To effectively perform the on-demand inverse design, we need to extract the required

Table 1. Dimensions chosen for the dataset preparation for predicting geometrical parameters of the metamaterial's cantilever resonator

Parameters $[ilde{ heta}]$	Domain of random values [m]
\tilde{b}_r	U(0.1,0.5)
\tilde{h}_r	U(0.005,0.02)
\tilde{l}_r	U(0.1,1.5)

geometrical features from the high-dimensional spectrum. The core task, therefore, becomes effective dimensionality reduction and feature extraction. This makes AEs an appropriate tool for this task. AEs excel at learning compressed representations of high-dimensional data using an encoder and are a powerful tool for feature extraction. Moreover, the decoder serves as a validator, ensuring that the result is meaningful and accurate. The advantages of AEs, which have been effectively demonstrated in various inverse design studies (Harper et al., 2020; Li et al., 2020; Gao et al., 2022), make the AE a robust and reliable choice for performing inverse design.

The AE architecture employed in this work comprises an encoder block, an intermediate layer, and a decoder block. The encoder maps the input data to a lower-dimensional representation while the decoder reconstructs the input from this compressed representation. The latent space, connecting the encoder and decoder, stores the essential features of the input data. In practice, the encoder network (\mathcal{B}) first extracts the important features from the given input layer $X \in \mathcal{R}$ to an abstract space, known as the latent space, as expressed by Mahesh et al. (2021).

$$\mathcal{H} = \mathcal{B}_{\phi}(X) \tag{7}$$

for $H \in \mathcal{R}$, ϕ being the collection of parameters of the encoder network, and X being the input samples. Then, the decoder model (\mathcal{D}) reverses the latent space to the reconstructed output layer X'. The output of the decoder is formulated as

$$X' = \mathcal{D}_{\theta}(\mathcal{H}) \tag{8}$$

where θ is the collection of all parameters of the decoder model. In this work, the AE is used to regenerate the required resonator receptance response $\hat{u}(\omega)$ from a desired receptance spectrum $u(\omega)$.

In this study, the encoder block receives the receptance spectrum from the ideal resonator as input, which is calculated to control the resonant frequency of a desired structure. It compresses this dynamic characteristic based on mass and stiffness parameters in the latent space. This latent space is designed to represent the geometrical parameters of the cantilever resonator beam, including length, width, height, and total mass (selected mass ratio and beam mass parameters). The intermediate layer, acting as an abstract expression, delivers the geometrical parameters of the resonator as output. The decoder then utilizes these geometrical properties to reconstruct the receptance response, effectively functioning as an evaluator. A custom loss function ensures the latent space captures the resonator's geometric properties. This function compares the latent space values with the actual values for each sample, calculates the MSE, and adds it to the reconstruction error, which is defined as the difference between the actual signal and the reconstructed signal obtained from the decoder as

$$\operatorname{Loss}\left(\theta_{i}, \hat{\theta}_{i}, \boldsymbol{u}_{i}, \hat{\boldsymbol{u}}_{i}\right) = \frac{1}{n} \sum_{i=1}^{n} \left|\theta_{i} - \hat{\theta}_{i}\right|^{2} + \gamma \cdot \frac{1}{n} \sum_{i=1}^{n} \left|\boldsymbol{u}_{i}(\omega) - \hat{\boldsymbol{u}}_{i}(\omega)\right|^{2}$$
(9)

where θ_i is the actual geometric parameters, $\hat{\theta}_i$ denotes the predicted geometric parameters by the encoder, n is the total number of samples, (u) is the targeted resonator's receptance frequency, and \hat{u} the predicted receptance calculated with the estimated parameters. The decoder also returns a reconstruction receptance response, which is used only for model training and validation. Furthermore, γ is the weighting coefficient for reconstruction loss set to 0.5 based

on empirical tuning to balance the geometric parameter error and the spectral reconstruction error.

This custom loss function updates the network hyperparameters and weights. The AE is inherently an unsupervised model due to the nature of the reconstruction loss, which is unsupervised. On the other hand, the prediction of geometrical properties is supervised because all the geometrical properties are known, and there are no unlabeled samples in the model's training. As a result, this modification converts the model into a supervised AE, allowing the model to incorporate knowledge of each sample's geometry. In this setup, the reconstruction loss acts as a regularizer to ensure that the predicted geometries are meaningful. Adjusting the number of layers, neurons in each layer, and other hyperparameters using this custom loss function helps increase accuracy while reducing computational complexity.

CNN-AE model architecture

Among the various types of architecture discussed in the literature for the model, each offers its advantages and disadvantages. FCLs are computationally efficient. Still, they lack the ability to capture the spatial or temporal relationships within sequential data, such as a receptance spectrum, as they treat each data point independently and are primarily suitable for regression problems. On the other hand, LSTMs are designed to handle temporal dependencies. However, in this problem, the features are embedded in the spatial patterns of the frequency rather than temporal sequences, which makes LSTMs computationally more expensive without offering a significant advantage. In contrast, CNNs are well-suited to capturing spatial and local features in data through the use of convolutional filters, making them a powerful and efficient tool for extracting the salient features from the receptance spectrum. Therefore, integrating CNNs into the AE architecture provides a robust and efficient model for the inverse design problem when frequency spectral signals are involved. Figure 4 demonstrates the representation of the inverse design architecture receiving the dynamic information of the primary structure for the final parameter estimation.

Convolutional filters are used in the encoder to extract features from the spectrum. Each convolutional layer is followed by a maxpooling layer to reduce the feature dimensions and increase efficiency. Then, these extracted features are flattened and passed to dense layers to predict the geometrical properties of the resonator. Three separate feature weighting modules are introduced to enhance the accuracy of the proposed model in predicting geometrical properties that yield a spectrum similar to the desired one. Each module consists of dense layers that output a scalar weight representing the value of each geometry. The output of these three modules is then concatenated in the latent space between the encoder and the decoder. The three values inside the latent space are then passed to the AE's decoder block. The decoder block's architecture is the reverse of the encoder block, reconstructing the spectrum with the given geometrical properties. Instead of using max pooling, upsampling layers are employed to increase the dimension of the feature map, allowing it to match the decoder's output with the original spectrum. A dropout is applied after each layer to increase the generality and prevent overfitting.

The architecture of this model is presented in Table 2. The CNN-AE consists of 6 1D-CNN layers with 15, 31, 63, 128, 256, and 512 filters and a kernel size of 3, followed by maxpooling layers. Four dense layers with 1,024, 512, 256, and 128 neurons are used, and the output of the FCLs is then passed

separately to three feature weighting modules, each consisting of 64, 32, 16, and 1 neurons. Finally, these three values are again concatenated and are the output of the encoder. As explained, the decoder architecture mirrors the encoder architecture in reverse. The hyperparameters chosen for the model are the rectified linear unit activation function for all layers and the Adam optimizer with Nesterov momentum (Nadam), which features a cyclic learning rate that helps the model avoid getting stuck in a local minimum. The model was trained with a batch size of 256 over 300 epochs.

The pseudocode (Table 1) illustrates the described process, which involves generating a dataset assuming the resonator's geometric parameters as random variables and utilizing the general CNN-AE inverse design scheme. The AE takes the receptance response of the resonator in the frequency range of 0–3 Hz as its input and produces the geometric features as its output. To achieve this, a convolution-based AE has been proposed to capture the important features of the spectrum and predict the geometrical properties that will result in a spectrum close to the desired one. The process was conducted on a Google Colaboratory platform, utilizing an NVIDIA Tesla T4 GPU with 12 GB of RAM. The model was implemented using the TensorFlow library compiled in Python.

Multi-resonator control design can be applied with the CNN AE model; however, it is recommended to train the DL model on datasets that span specific frequency bands corresponding to the multiple modes of interest in uncoupled conditions, as per modal analysis theory. This enables the model to capture dynamic interactions effectively without incurring a significant loss of accuracy. Such an approach is particularly beneficial when deploying resonators tuned to different modal frequencies. As a general guideline, we suggest adopting a modular, uncoupled configuration for model training, unless the application specifically benefits from resonator coupling. This strategy improves model efficiency and ensures reliable vibration attenuation of the targeted frequency range.

Sensitivity optimization method

The inverse design workflow proposed in this paper integrates a CNN-AE with the sensitivity-based optimization procedure, creating a robust framework. Sensitivity-based optimization enhances the correlation between observed data and the model predictions (Friswell and Mottershead, 1995). This correlation is assessed using a cost function derived from the dynamic response data, which usually represents nonlinear functions of the model parameters. As a result, a repetitive process is employed. The success of this optimization approach directly depends on the initial guess for the parameter values to be estimated, as these significantly influence the convergence and associated challenges.

The CNN-AE provides the initial parameters required as input for the sensitivity-based method. This integration ensures that the optimization process begins with a closer approximation of the parameters, while the sensitivity method fine-tunes these optimized parameters. Consequently, the present approach offers an efficient model for rapidly designing dynamic controllers on demand, customized to the dynamic system's requirements. The dataset of the receptance response is obtained from the ideal desired control, which is assembled into a matrix expressed by $\mathbf{z} = [\mathbf{u}_1, \mathbf{u}_2, ..., \mathbf{u}_n]^T$. Penalty function methods generally use a truncated Taylor series expansion of the dynamic response data in terms of the unknown parameters, often limited to the first two series terms, yielding the linear approximation as Friswell and Mottershead (1995).

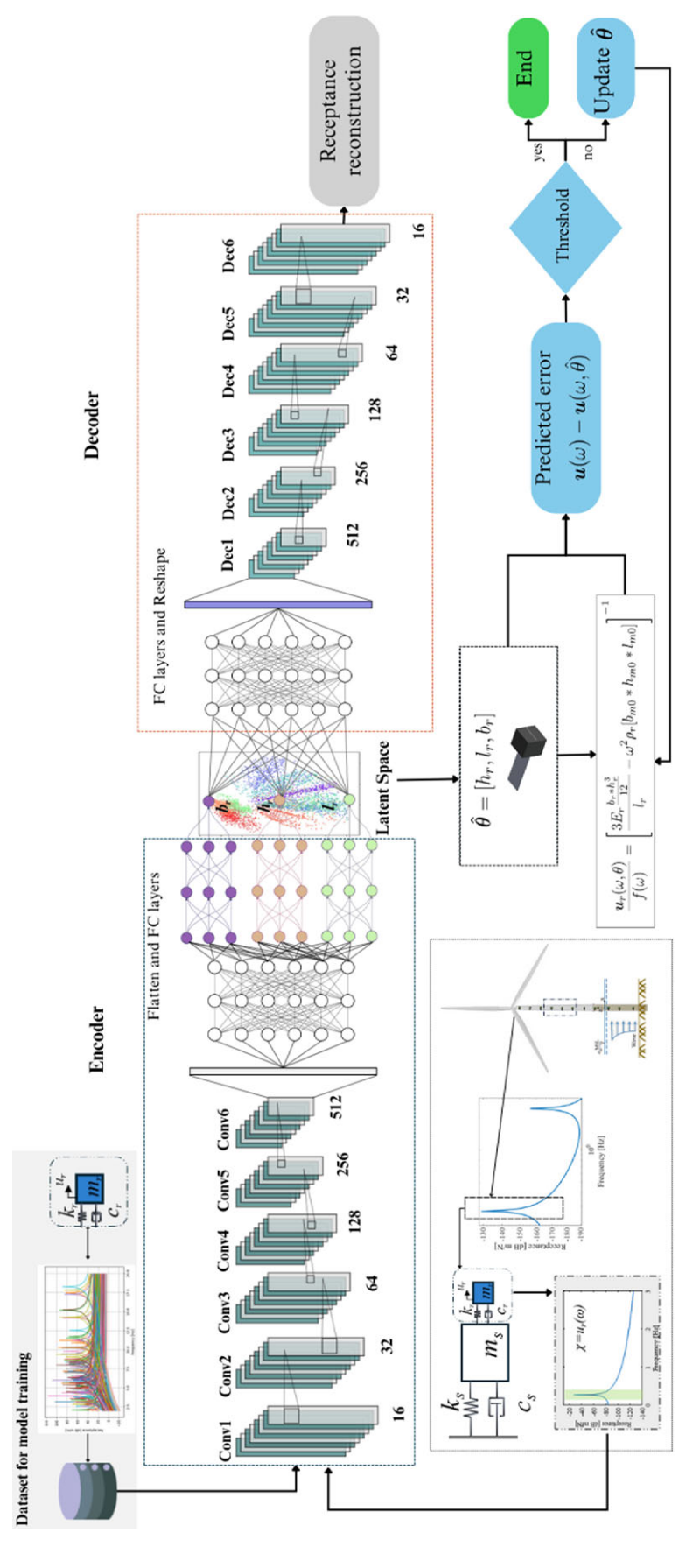


Figure 4. Schematic representation of inverse design architecture.

Table 2. CNN-autoencoder inverse design model description. Output 1 predicts geometrical parameters, and Output 2 exhibits the receptance reconstruction

Encoder				Decoder			
Layer	Output shape	Parameters	Layer	Output shape	Parameters		
Input layer	(None, 512, 1)	0	Input layer	(None, 3)	0		
Conv1D	(None, 512, 16)	64	Dense	(None, 128)	512		
Dropout	(None, 512, 16)	0	Dropout	(None, 128)	0		
MaxPooling1D	(None, 256, 16)	0	Dense	(None, 256)	33,024		
Conv1D	(None, 256, 32)	1,568	Dropout	(None, 256)	0		
Dropout	(None, 256, 32)	0	Dense	(None, 512)	131,584		
MaxPooling1D	(None, 128, 32)	0	Dropout	(None, 512)	0		
Conv1D	(None, 128, 64)	6,208	Dense	(None, 1024)	525,312		
Dropout	(None, 128, 64)	0	Dropout	(None, 1024)	0		
MaxPooling1D	(None, 64, 64)	0	Dense	(None, 4096)	4,198,400		
Conv1D	(None, 64, 128)	24,704	Dropout	(None, 4096)	0		
Dropout	(None, 64, 128)	0	Reshape	(None, 8, 512)	0		
MaxPooling1D	(None, 32, 128)	0	Conv1D	(None, 8, 512)	786,944		
Conv1D	(None, 32, 256)	98,560	Dropout	(None, 8, 512)	0		
Dropout	(None, 32, 256)	0	UpSampling1D	(None, 16, 512)	0		
MaxPooling1D	(None, 16, 256)	0	Conv1D	(None, 16, 256)	393,472		
Conv1D	(None, 16, 512)	393,728	Dropout	(None, 16, 256)	0		
Dropout	(None, 16, 512)	0	UpSampling1D	(None, 32, 256)	0		
MaxPooling1D	(None, 8, 512)	0	Conv1D	(None, 32, 128)	98,432		
Flatten	(None, 4096)	0	Dropout	(None, 32, 128)	0		
Dense	(None, 1024)	4,195,328	UpSampling1D	(None, 64, 128)	0		
Dropout	(None, 1024)	0	Conv1D	(None, 64, 64)	24,640		
Dense	(None, 512)	524,800	Dropout	(None, 64, 64)	0		
Dropout	(None, 512)	0	UpSampling1D	(None, 128, 64)	0		
Dense	(None, 256)	131,328	Conv1D	(None, 128, 32)	6,176		
Dropout	(None, 256)	0	Dropout	(None, 128, 32)	0		
Dense	(None, 128)	32,896	UpSampling1D	(None, 256, 32)	0		
Dense (3X)	(None, 64)	8,256	Conv1D	(None, 256, 16)	1,552		
Dropout (3X)	(None, 64)	0	Dropout	(None, 256, 16)	0		
Dense (3X)	(None, 32)	2,080	UpSampling1D	(None, 512, 16)	0		
Dropout (3X)	(None, 32)	0	Output 2	(None, 512, 1)	49		
Dense (3X)	(None, 16)	528					
Dropout (3X)	(None, 16)	0					
Dense (3X)	(None, 1)	17					
Dropout (3X)	(None, 1)	0					
Multiply (3X)	(None, 128)	0					
Concatenate	(None, 384)	0					
Output 1	(None, 3)	1,155					

$$\delta \mathbf{z} = \mathbf{S}_{j} \delta \hat{\boldsymbol{\theta}}, \tag{10}$$

where $\delta \mathbf{z} = \mathbf{z}_m - \mathbf{z}_j$ represents the error in the output, $\delta \hat{\theta} = \hat{\theta} - \hat{\theta}_j$ signifies the perturbation in the parameters, and \mathbf{S}_j denotes the sensitivity matrix that includes the derivatives of the response

associated with the parameters $\hat{\theta}_j$. Given that there are more data points than unknown parameters, Eq. (10) results in an overdetermined set of simultaneous equations that can be addressed using a least squares solution. By implementing the penalty function

$$J\left(\delta\hat{\theta}\right) = \varepsilon^{T}\varepsilon,\tag{11}$$

where $\varepsilon = \delta \mathbf{z} - \mathbf{S}_j \delta \hat{\theta}$ is the error in the predicted measurements based on the updated parameters. Substituting Eq. (11) in Eq. (10) leads to

$$J(\delta\hat{\theta}) = \delta \mathbf{z}^T \delta \mathbf{z} - 2\delta\hat{\theta}^T \mathbf{S}_j^T \delta \mathbf{z} + \delta\hat{\theta}^T \mathbf{S}_j^T \mathbf{S}_j \delta\hat{\theta}.$$
 (12)

Minimizing *J* in relation to $\delta \hat{\theta}$ is equivalent to

$$\nabla J\left(\delta\hat{\theta}\right) = 0 = -\mathbf{S}_{j}^{T}\delta\mathbf{z} + \mathbf{S}_{j}^{T}\mathbf{S}_{j}\delta\hat{\theta},\tag{13}$$

and solving Eq. (13) for $\delta \hat{\theta}$ results in $\delta \hat{\theta} = \left[\mathbf{S}_j^T \mathbf{S}_j \right]^{-1} \mathbf{S}_j^T \delta \mathbf{z}$, and the updated parameter can be obtained as

$$\hat{\theta}_{j+1} = \hat{\theta}_j + \left[\mathbf{S}_j^T \mathbf{S}_j \right]^{-1} \mathbf{S}_j^T \left(\mathbf{z}_m - \mathbf{z}_j \right). \tag{14}$$

The updated parameters are the output of the inverse design process, which accurately matches the dynamic design criteria.

Numerical results

Attenuating vibrations in the low-frequency range (0–3 Hz) is challenging due to the physical limits of resonator-based metastructures integrated into primary structures. Our work addressed this challenge and validated effective low-frequency attenuation, as detailed in Machado et al. (2024) and Machado and Dutkiewicz (2025). The embedded metastructure, tuned to the wind turbine's first resonant mode, outperforms classical tuned mass dampers. Although the attenuation band is narrow due to modal constraints, the targeted reduction at critical frequencies shows practical benefits. The metamaterial solution also reduces controller size compared to tuned mass damper (TMD) and removes the need for precise placement, offering greater integration flexibility. Therefore, an effective physical design of the controllers is still an open issue. This article presents a numerical analysis that includes a sensitivity assessment of the

controller's parameters, an evaluation of the proposed AE inverse networks' efficiency, and an investigation into the efficacy of the on-demand resonator's design in the metamaterial turbine for achieving the desired dynamic characteristics.

Dynamic and stochastic analysis of the resonators

The resonator's dynamic responses in frequency, time domain, and phase plane diagrams of the structural response are examined for the controller, assuming an undamped resonator, as shown in Figure 5a–d, and a resonator with additional hysteretic damping incorporated into its stiffness, as shown in Figure 5e–g. The resonator control system consists of a single-degree-of-freedom mass-spring-damping system. The mass is assumed to be 10% of the turbine's mass.

The natural frequency characteristics of the dynamic vibration resonator, as described in Eq. (3), are determined by its stiffness and mass. Consequently, in its fundamental geometric form, the physical resonator is assumed to be a cantilever beam connected to a lumped mass. The beam elements represent the stiffness (k_r) , while the combined beam and lumped masses $(l_{m0}, b_{m0}, h_{m0}, m_0)$ represent the mass. The geometric dimensions of the beam, specifically its b_r, l_r , and h_r , are then determined by the CNN-AE inverse design approach, which enables the determination of the resonator's parameters that match the desired dynamic response. Hence, the desired resonator receptance spectra are assumed to be the CNN-AE input data corresponding to a collection of the three geometric parameters of the resonators.

The random values of the geometrical parameters are generated using both LHS and Monte Carlo techniques, and their PDFs are shown in Figure 6. As can be seen, the parameters generated with the LHS exhibit a more uniform distribution across each parameter range compared to the Monte Carlo technique. This uniform distribution will inform the model with values from all over the design space, rather than redundant values, which will prevent the model from being biased toward a specific region and promote more robust training.

DL models often provide only point predictions, lacking information about their accuracy, sampling errors, and reliability

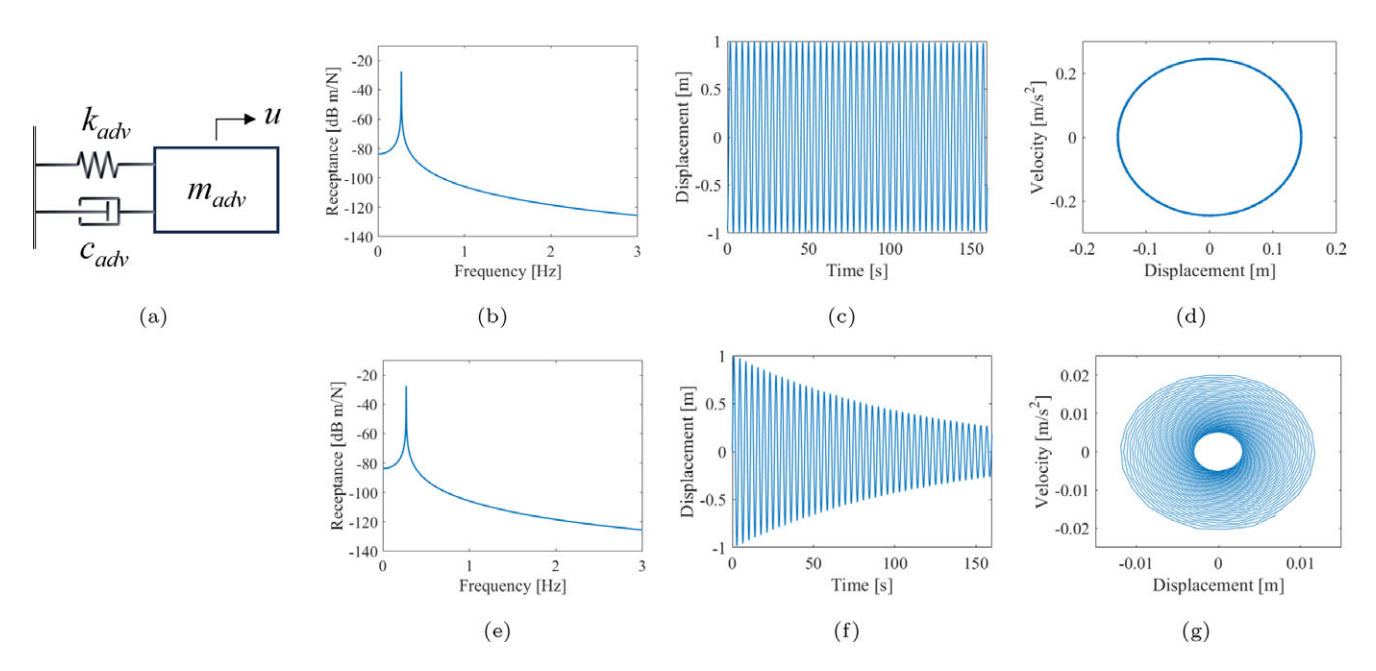


Figure 5. Resonator representation, receptance response, temporal, and phase diagram responses for (a–d) undamped resonator and (e–g) resonator with hysteretic damping of 0.01 of the damping factor.

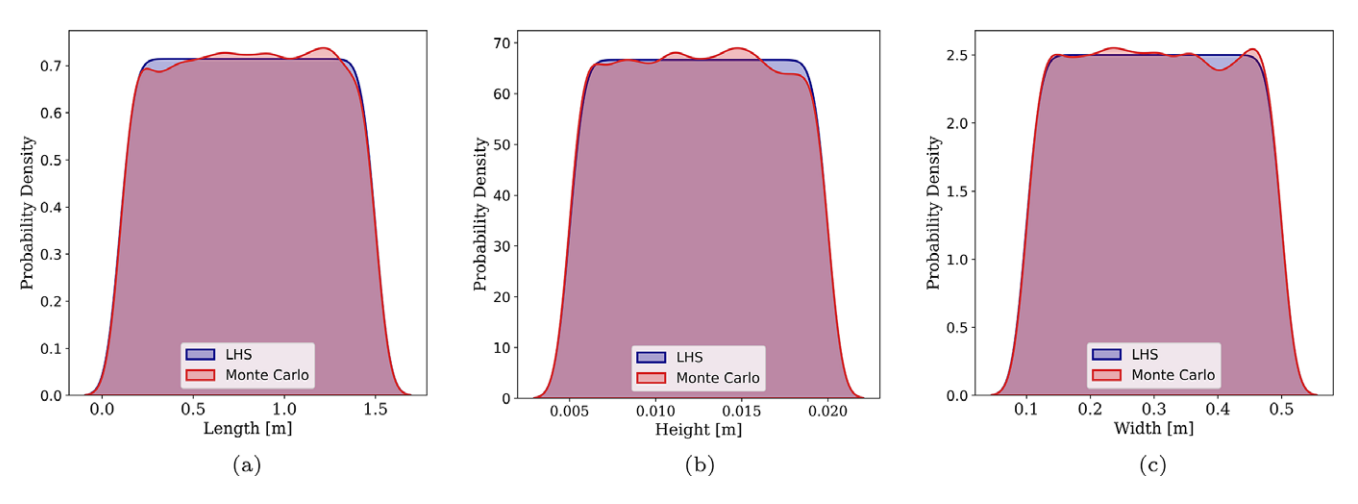


Figure 6. Comparison of probability density functions for the geometric parameters: (a) length, (b) height, and (c) width, under LHS versus the Monte Carlo technique.

(Khosravi et al., 2011; Lu et al., 2024). These models typically learn the mapping between inputs and target variables, producing deterministic estimates of the relationship. However, when dealing with multivalued targets or sparse data, the average outputs of the models may not accurately represent the true target. To enhance the reliability of DL decision-making, it is crucial to quantify the uncertainty associated with predictions, models, and datasets. This enables an accurate assessment and qualification of the predictions' accuracy and risk, ultimately enhancing the overall reliability and credibility of DL methods. Hence, sensitivity analysis of the random parameters and the uncertainty propagation to the resonators' dynamic response are explored in Figures 7 and 8. The influence of each random variable on the dynamic response is presented in Figure 7, which shows samples of the receptance response at the top and the ensemble mean, along with the 90% confidence interval below. Specifically, Figure 7a illustrates the resonator's receptance response, where the beam's length is the only random variable, while the other parameters are kept deterministic. Figure 7b considers the beam's width as a random variable, Figure 7c considers the height, and Figure 7d assumes all three variables are random. Variability in length has the most significant impact on the shift in resonant peaks, followed by changes in height and width. The response amplitude is shown to be more sensitive to the length

parameter. Combining all three random variables yields a significant frequency shift, with the amplitude decreasing at higher frequencies.

The probability density function (PDF) calculated using the resonant frequency and corresponding amplitude values is presented in Figure 8a and b, respectively. In both cases, when considering the length as a random variable, the PDF graphs exhibit a bimodal statistical behaviour, with the primary statistical mode appearing as ragged histogram shapes around the frequencies of interest. The PDF assumes an unimodal statistical shape for both resonant frequency and amplitude values when considering the width and height as random variables. The random length causes a large dispersion with lower amplitude, while the random width results in a narrow and high-density distribution. The height PDF shows a medium amplitude spread density around the target frequency. The PDFs illustrate the random contribution of each variable to the resonator's dynamic response, with resonant frequencies predominantly influenced by length parameters. The PDFs for resonant frequency and amplitude, considering the combination of all three random variables, are displayed in Figure 8c and d. The merged random variables yield a unimodal statistical distribution in the resonator's dynamic response, reflecting the combined characteristics of the random variables, including bandwidth and amplitude. In practice, these random variables are

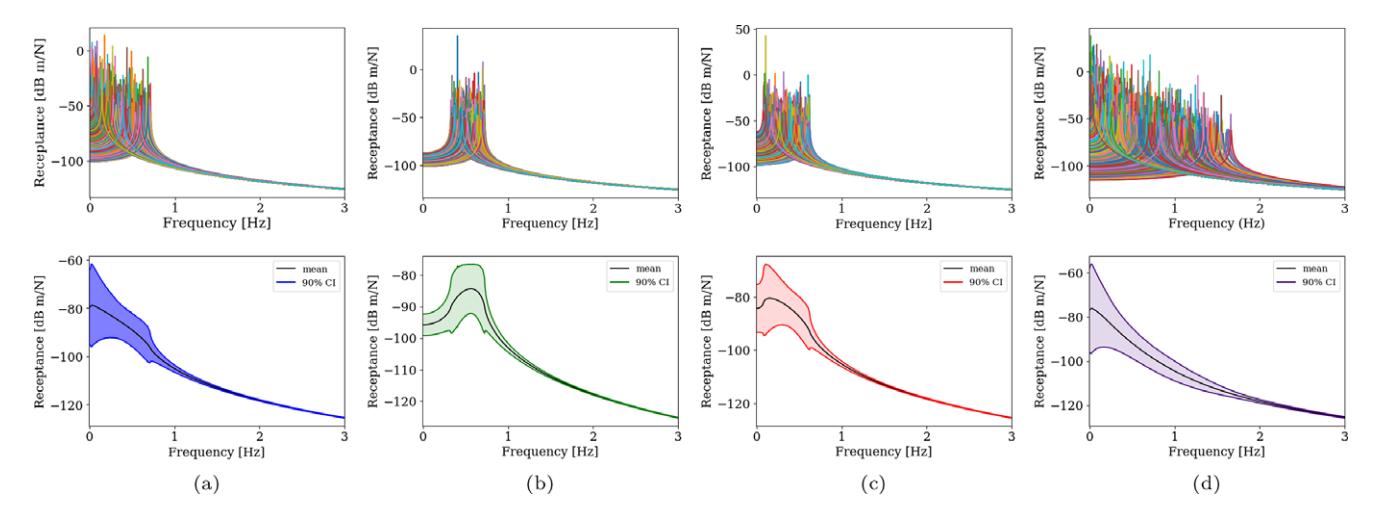


Figure 7. Receptance response of the resonator, assuming as random variables the beam (a) length, (b) width, (c) height, and (d) the three variables.

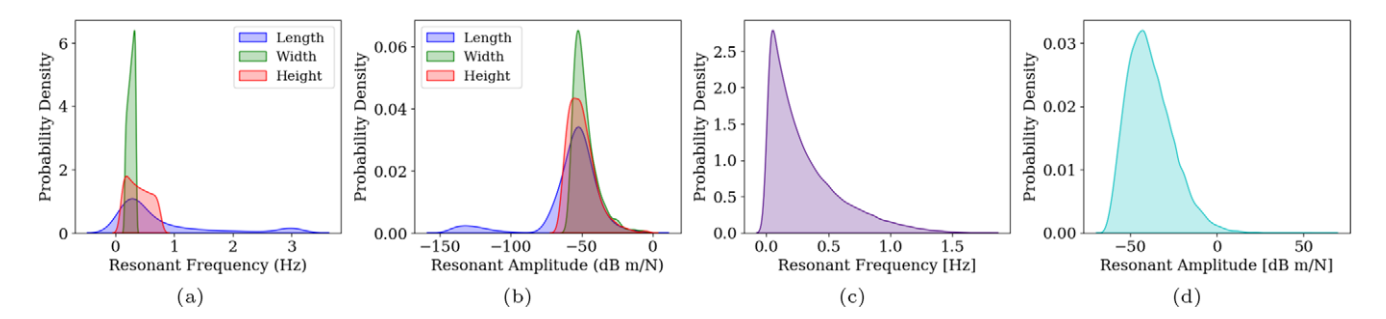


Figure 8. Probability density function calculated with the resonant frequency and respective amplitude values estimated for each sample. (a) PDF of the resonant frequency assuming random variable length (blue), width (green), and height (red). (b) PDF of the resonant amplitude assuming random variable length (blue), width (green), and height (red). (c) PDF of the resonant frequency and (d) PDF of the resonant amplitude, assuming the three random variables simultaneously.

assumed to sample the dataset used in the CNN-AE inverse design. Understanding the influence of each parameter in the dynamic system is crucial for accurately evaluating the results.

Inverse design of the metamaterial's resonator

The wind turbine metastructure is designed to control its first resonant frequency as proposed by Machado et al. (2024). The following section addresses the inverse design of the physical resonators of the metaturbine using the proposed framework. In the inverse model, 10% of the dataset is allocated for testing purposes. In practice, the CNN-AE model maps the relationship between the resonator's receptance response and its target parameters, which are the output of the encoder network in the latent space, in such a way that the predicted geometries generate a spectrum similar to the desired one. Notably, the identification of attributes in inverse design is executed in a supervised way.

The interaction between the host structure and the resonator is considered only in the numerical model used to evaluate control performance, not during the inverse design step, which is intentionally formulated as a data-driven process for practical application. This interaction is idealized via the test step using the turbine numerical model, which, in this study, is based on a spectral model but is not limited to it. Since the resonator position and mass ratio

are preestablished, following the metastructure concept, the control frequency remains constant, unlike in classical TMD designs, where location tuning is essential and directly influences the system's dynamic characteristics. Therefore, parametric fine-tuning, if necessary, is addressed by recalculating the resonator geometry using sensitivity-based methods in an automatic procedure.

Within the dataset, many spectra exhibit identical shapes and resonance frequencies, although each is generated from different combinations of geometrical parameters. This research aims to identify specific geometric configurations that produce a desired spectrum, accepting any predicted values that fall within the predefined domain as described in Table 1. Thus, more than a single solution is expected for each spectrum. Four samples are randomly selected from the test data, and the corresponding values of the actual and predicted geometries are used in Eq. (5), which calculates the corresponding spectrum for each case.

Table 3 presents the actual, predicted, and updated geometrical parameters, along with their corresponding resonance frequencies for each sample. Figure 9 illustrates the generated spectrum based on the actual, predicted, and updated geometries, where applicable. For the first two samples, Figure 9a and b, the difference between the actual and predicted resonance frequencies and receptance responses is less than the threshold (0.02 Hz). For the first sample, the difference is 0.004 Hz, and for the second one, it is 0.011 Hz.

Table 3. Actual and predicted geometric parameters, RMS values, resonance frequencies, and errors for four randomly selected samples

		Sample 1		Sample 2		
Parameter	Actual	Predicted	Updated	Actual	Predicted	Updated
Length [m]	0.178	0.183	-	0.986	1.222	-
Width [m]	0.484	0.266	_	0.415	0.357	-
Height [m]	0.006	0.009	-	0.019	0.016	-
RMS [dB]	109.568	109.565	-	109.551	109.552	-
Resonance frequency [Hz]	0.011	0.015	-	0.827	0.816	-
	Sample 3		Sample 4			
		Sample 3			Sample 4	
	Actual	Sample 3 Predicted	Updated	Actual	Sample 4 Predicted	Updated
Length [m]	Actual 0.669	· · · · · · · · · · · · · · · · · · ·	Updated	Actual 0.941	<u> </u>	Updated 0.756
Length [m] Width [m]		Predicted	<u> </u>		Predicted	<u> </u>
	0.669	Predicted 0.992	1.019	0.941	Predicted 0.793	0.756
Width [m]	0.669 0.282	0.992 0.303	1.019	0.941 0.453	0.793 0.304	0.756

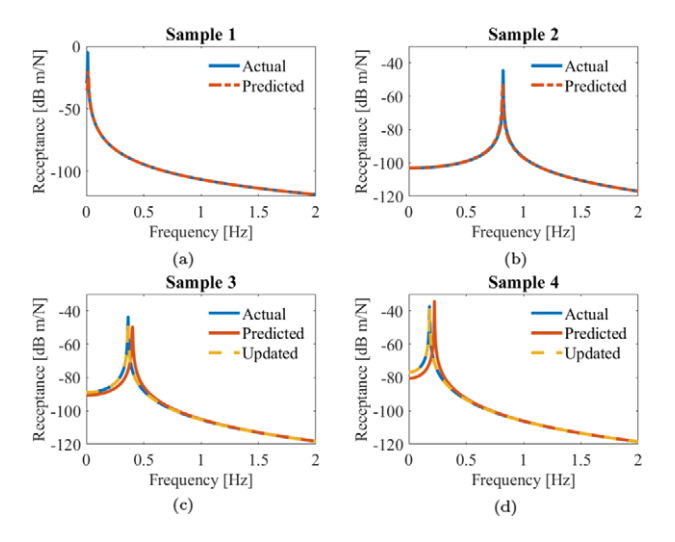


Figure 9. Resonator's receptance response of the randomly selected samples, calculated with Eq. (5) using the estimated parameter given by the encoder. The four samples' parametric features are given in Table 3.

This level of accuracy meets the preestablished design criteria. However, for the third and fourth samples (Figure 9c and d), the difference surpasses the acceptable error threshold. For the third sample, the difference is 0.053 Hz, and for the fourth sample, the difference is 0.047 Hz. In these cases, the predicted parameters are refined through the sensitivity optimization procedure. After the optimization, the updated parameters achieve the desired resonance frequency with minimal error, and the corresponding receptance spectrum closely matches the target. The model's efficiency is evaluated based on its ability to predict parameters that yield a spectrum with a resonance frequency near the desired value, ensuring accurate and effective controller performance.

The CNN-AE consistently provides initial estimations of dynamic characteristics that are close to the desired values. For samples with higher prediction errors, the model fine-tunes the parameters to satisfy the design criteria. Because the CNN-AE generates estimates near the target geometrical parameters, the optimization procedure is highly efficient, requiring only a few seconds to compute the optimized parameters. Although the training of the model took ~2 h, the trained model can predict the geometrical properties of the desired spectrum in under a second. As a result, the inverse on-demand physical resonator design process is remarkably fast, taking less than 2 min even when optimization is necessary.

It is important that the model's prediction results in a spectrum similar to the desired one. To further evaluate the model's prediction, the resonance frequency of the actual spectrum is compared with the predicted one for all samples in the test dataset. The performance metrics for this comparison are an MSE (Mean Squared Error) of 0.0021, an MAE (Mean Absolute Error) of 0.0415, and an R^2 of 0.975. The model performed well across all metrics. Low values, tending toward zero, of MSE and MAE indicate small deviations between the predicted and actual resonance frequencies. Furthermore, a value of \mathbb{R}^2 close to 1 indicates that the model explains a significant portion of the variance in the data. Moreover, a representation of the overall energy in a spectrum can be calculated by the signal's mean root square (RMS), which often represents the overall energy level. The RMSs of the actual and predicted spectra of each sample have also been compared for the entire test data set, and the results for both the resonance frequency and the RMS are depicted in Figure 10.

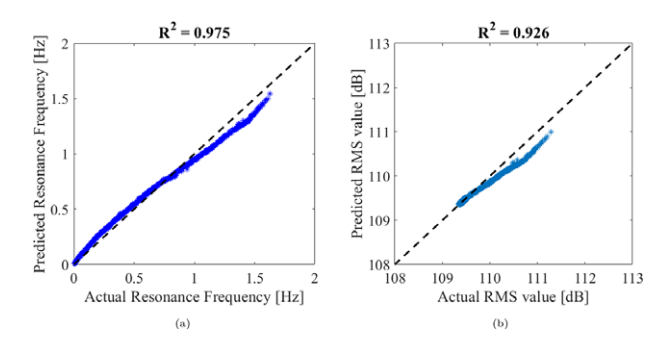


Figure 10. Comparison of (a) resonance frequency and (b) RMS values for the test samples.

On-demand inverse design of the metamaterial wind turbine

Section "Inverse design of the metamaterial's resonator" illustrates the performance of the model in predicting samples from the test dataset, demonstrating that the proposed model's versatility encompasses the input of any spectrum within the training range and can predict the resonator's geometrical parameters. This section demonstrates the effectiveness of inverse design for different wind turbine metastructure local resonator simulations in an on-demand design and simulations of an industrial application. The base turbine numerical model relies on the monopile NREL 5 MW offshore virtual wind turbine (Jonkman et al., 2009; Jonkman and Musial, 2010) and numerical modeling in Machado et al. (2024). The resonators are periodically placed along the tower of the wind turbine, as illustrated in Figure 1. The forward design of the turbine controller assumes the target frequency and designs the ideal dynamic resonator, considering only the mass ratio and stiffness. Therefore, in practical application, the physical controllers assume a geometry and value that follows their dynamic idealization. Thus, in this analysis, the inverse design of the turbine metamaterial relies on estimating the resonator's physical geometries using the proposed model.

The first resonant frequency of the wind turbine varies between 0 and 2 Hz, so the trained model is suitable for such an analyst without the need to retrain the model. Three different turbines, each with its respective resonant frequencies and features, are described in Table 4. To evaluate this approach, three different target spectra are fed into the proposed model, with resonance frequencies of 0.27 Hz for Case 1, 0.34 Hz for Case 2, and 0.5 Hz

Table 4. Resonator properties before and after fine-tuning for three cases

Case	Parameter	Predicted	Fine-tuned
Case I: Target 0.27 Hz	Length (m)	0.920	0.89
	Width (m)	0.299	0.268
	Height (m)	0.012	0.011
	Resonance frequency (Hz)	0.31	0.27
Case II: Target 0.34 Hz	Length (m)	0.977	0.948
	Width (m)	0.301	0.275
	Height (m)	0.013	0.012
	Resonance frequency (Hz)	0.39	0.34
Case III: Target 0.5 Hz	Length (m)	1.085	1.077
	Width (m)	0.310	0.303
	Height (m)	0.014	0.014
	Resonance frequency (Hz)	0.52	0.50

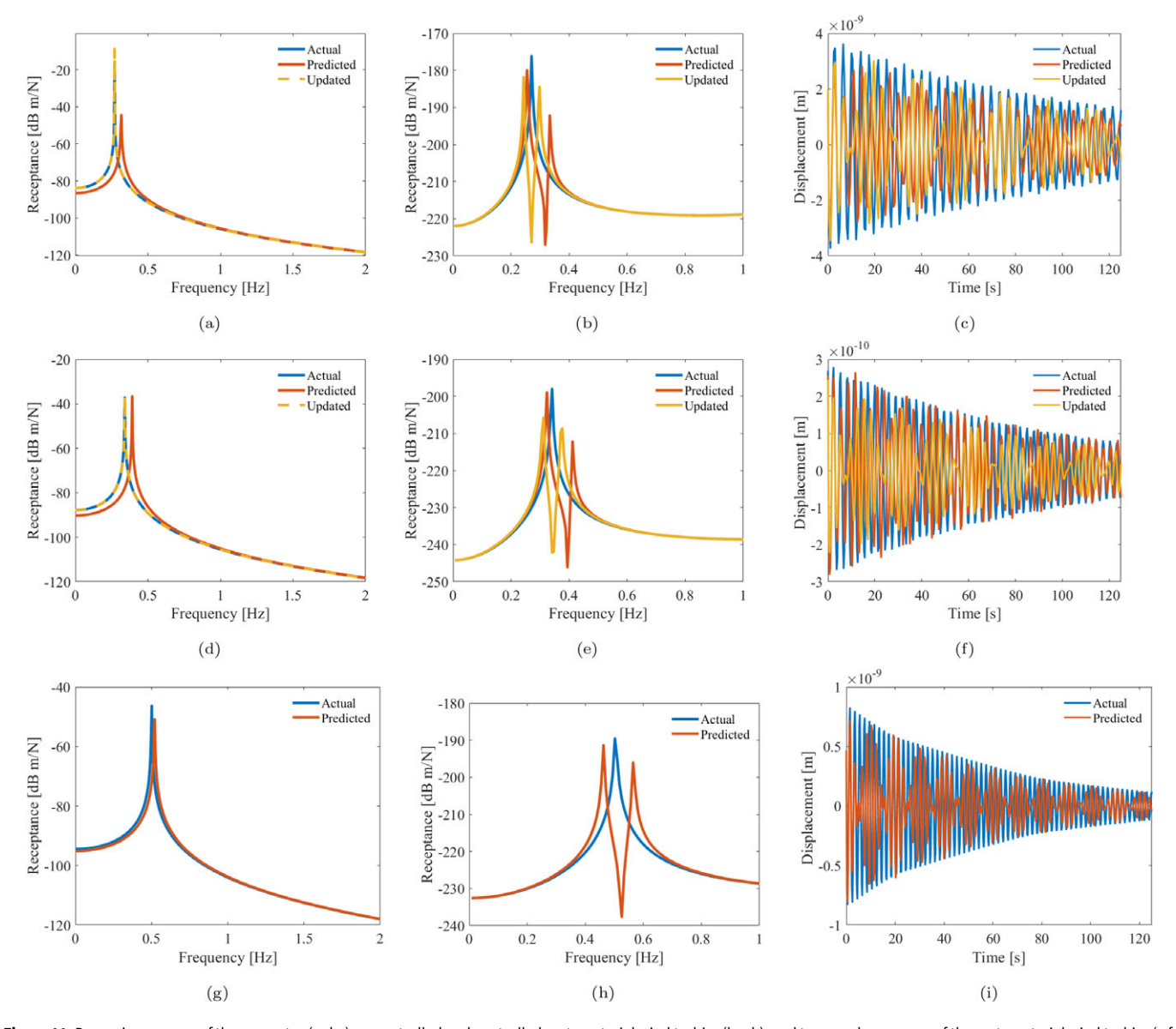


Figure 11. Dynamic response of the resonator (a,d,g), uncontrolled and controlled metamaterial wind turbine(b,e,h), and temporal responses of the metamaterial wind turbine(c,f, i) of the cases described in Table 4. (a,b,c) illustrate Case I, (d,e,f) illustrate Case II, and (g,h,i) illustrate Case III.

for Case 3. Each case is associated with values for the predicted and updated resonator's length, width, height, and resonance frequency.

Figure 11a, d, g compares the target receptance of the resonator, calculated using the dynamic analytical expression, with the spectrum predicted by the CNN-AE model and the updated signal using the sensitivity optimization updating technique. The CNN-AE model's parameter predictions show spectra that are near the actual ones in Cases I (a) and II (d), and match within an acceptable error in Case III (c). In Case I, the resonance frequency of the target spectrum is 0.27 Hz, while the model predicts 0.31 Hz. Similarly, in Case II, the target frequency is 0.34 Hz, but the predicted frequency was 0.39 Hz. Due to these errors, parameter updates are required for accurate design. In Case III, the target resonance frequency is 0.50 Hz, and the model predicts 0.52 Hz. The error is minimal, so fine-tuning is optional. Overall, the initial predictions of the model are quite accurate. Since precise frequency alignment is crucial for effective on-demand vibration control, in cases where a significant

discrepancy exists between the desired resonance frequency and the signal, parameter updating is employed.

The interaction between the resonators and the primary structure leads to a division in the controlled resonance mode, which results in extra degrees of freedom near the targeted mode shape. As a result, additional resonance frequencies appear on either side of the system's operating frequency, which the resonators are designed to control. Although this passive vibration control technique has a clearly defined range of effectiveness, exceeding this range can lead to negative effects, such as increasing the amplitudes of neighboring modes. Figure 11b,e,h shows the receptance, and Figure 11c,f,i shows the temporal responses of the uncontrolled turbine under unitary excitation, the controller turbine assuming the predicted and updated parameters in the resonator design, where the predicted and updated parameters are listed in Table 4.

In all cases, it is a respected split of the target frequency with a symmetric attenuation bandwidth. In Cases I and II, the resonators using predicted parameters induce an asymmetric frequency split, which is optimized and corrected using updated parameters. Overall, the physical resonator inverse designs by the proposed model demonstrate effective vibration mitigation performance for the metamaterial turbine, closely following the ideal dynamic resonator. In practice, the physical control is installed in the primary structure, where some inherent variability is expected, as predicted by the model, which can be rapidly recalculated to deliver an accurate geometry associated with the design requirement. The inverse design model proves to be a precise and viable alternative for modeling and designing vibration controllers with good precision and parametric prediction guidance.

Conclusion

This study presented an innovative methodology for the inverse design of passive vibration controllers tested to design a local resonator of a wind turbine metastructure and evaluate its interaction with host structure control performance. The CNN-AE model is guided by a physics-informed approach to improve the on-demand inverse design processes, showing significant potential in optimizing metastructure manufacture. The CNN-AE was developed to efficiently estimate the geometric parameters of physical passive controllers from dynamic response data, yielding the estimated geometric parameters and the receptance spectrum of the designed resonator as its output. The proposed model demonstrated excellent predictive accuracy, even at very low frequencies. Furthermore, statistical evaluations of uncertainty and parameter variability provided valuable insights into the design's robustness and performance under varying conditions.

In practical applications, the CNN-AE inverse design approach enables a fast and efficient determination of resonator geometries, specifically the local resonator of the wind turbine's metastructure, thereby facilitating the implementation of effective vibration control for complex systems, not limited to this system. The comparison of ideal versus physically designed resonators indicates that the proposed model can achieve vibration mitigation performance that closely matches expectations. This underscores the potential of DL methods to enhance the design and optimization of structural components in real-world engineering applications. Future research will explore the integration of more complex dynamical models, a topological representation of the metastructure, and broader datasets to refine the accuracy of CNN-AE designs. Additionally, investigating the scalability of these methods for largescale systems and varying operational conditions will be crucial to advancing the practical deployment of vibration control systems in diverse engineering contexts. This study establishes a solid foundation for advanced ML techniques to design and optimize vibration control systems with precision and efficiency based on their dynamic behavior.

Data availability statement. The data and code supporting the findings of this study are available in https://zenodo.org/communities/swintproject.

Funding statement. This research is part of the project number 2022/45/P/ST8/02123, co-funded by the National Science Centre and the European Union Framework Programme for Research and Innovation Horizon 2020 under the Marie Skłodowska-Curie grant agreement number 945339.

M.R.M. acknowledges the sponsors of projects (CNPq.404013/2021-0 and 444595/2024-4, Capes 001, and FAPDF.00193-00002143/2023-02).

Competing interests. The authors declare none.

References

- Amirkulova FA, Zhou L, Abbas A, Lai P, Qiu C and Shah TA (2022) Acoustic metamaterial design framework using deep learning and generative modeling. The Journal of the Acoustical Society of America. https://doi.org/10.1121/ 10.0011233
- Ariza M, Conti S, Ortiz M (2024) Homogenization and continuum limit of mechanical metamaterials, *Mechanics of Materials* 196 105073. https://doi. org/10.1016/j.mechmat.2024.105073. https://www.sciencedirect.com/science/ article/pii/S0167663624001650
- Ashalley E, Acheampong KN, Besteiro L, Yu P, Neogi A, Govorov A and Wang ZM (2020) Multitask deep-learning-based design of chiral plasmonic metamaterials. *Photonics Research* 8, 1213–1225. https://doi.org/10.1364/prj.388253.
- Brennan MJ, Some recent developments in adaptive tuned vibration absorbers/ neutralisers, Shock and Vibration 13 (4–5) (2006) 531–543. https://doi. org/10.1155/2006/563934.
- Brown NK, Garland AP, Fadel GM and Li G (2023) Deep reinforcement learning for the rapid on-demand design of mechanical metamaterials with targeted nonlinear deformation responses. *Engineering Applications of Artificial Intelligence* 126, 106998. https://doi.org/10.1016/j.engappai.2023.106998.
- Cerniauskas G and Alam P (2023) Tensile properties of 3d-projected 4-polytopes: A new class of mechanical metamaterial. *Advanced Engineering Materials* 25 (17), 2300251. https://doi.org/10.1002/adem.202300251.
- Cerniauskas G, Sadia H and Alam P (2024) Machine intelligence in metamaterials design: A review. Oxford Open Materials Science 4. https://doi.org/10.1093/oxfmat/itae001.
- Chen J, Chen Y, Xu X, Zhou W and Huang G (2022) A physics-guided machine learning for multifunctional wave control in active metabeams. Extreme Mechanics Letters 55, 101827. https://doi.org/10.1016/j.eml.2022.101827.
- Chen Y, Zhu J, Xie Y, Feng N and Liu Q (2019) Smart inverse design of graphene-based photonic metamaterials by an adaptive artificial neural network. *Nanoscale* 11 19, 9749–9755. https://doi.org/10.1039/c9nr01315f.
- Cho MW, Hwang SH, Jang J-Y, Hwang S, Cha KJ, Park DY, Song K and Park SM (2024) Beyond the limits of parametric design: Latent space exploration strategy enabling ultra-broadband acoustic metamaterials. *Engineering Applications of Artificial Intelligence* 133, 108595. https://doi.org/10.1016/j.engappai.2024.108595.
- Cleante V, Brennan M, Gonçalves P, Carneiro Jr JP, Carneiro Jr J, On the formation of a super stop-band in finite mono-coupled periodic structures using an array of vibration absorbers: Controlling parameters and physical insight, *Mechanical Systems and Signal Processing* **180** (2022) 109383. https://doi.org/10.1016/j.ymssp.2022.109383.
- Coelho JS, Machado MR, Dutkiewicz M and Teloli RO (2024) Data-Driven Machine Learning for Pattern Recognition and Detection of Loosening Torque in Bolted Joints. https://doi.org/10.1007/s40430-023-04628-6
- Colherinhas GB, de Morais MVG and Machado MR (2022) Spectral model of offshore wind turbines and vibration control by pendulum tuned mass dampers. *International Journal of Strucutral Stability and Dynamics* 22 (05). https://doi.org/10.1142/S0219455422500535.
- Dalela S, Balaji PS and Jena DP (2022) A review on application of mechanical metamaterials for vibration control. Mechanics of Advanced Materials and Structures 29 (22), 3237–3262. https://doi.org/10.1080/15376494.2021.1892244.
- de Moura B, Machado M, Dey S and Mukhopadhyay T (2024) Manipulating flexural waves to enhance the broadband vibration mitigation through inducing programmed disorder on smart rainbow metamaterials. Applied Mathematical Modelling 125, 650–671. https://doi.org/10.1016/j.apm.2023.10.011.
- Dedoncker S, Donner C, Taenzer L and Damme BV (2023) Generative Inverse Design of Multimodal Resonant Structures for Locally Resonant Metamaterials
- Donda K, Zhu Y, Merkel A, Fan S-W, Cao L, Wan S and Assouar B (2021) Ultrathin acoustic absorbing metasurface based on deep learning approach. Smart Materials and Structures 30 (8). https://doi.org/10.1088/1361-665X/ac0675.
- Dutkiewicz M, Machado MR (2019a) Spectral approach in vibrations of overhead transmission lines, IOP Conference Series: Materials Science and Engineering 471 Session 4. https://doi.org/10.1088/1757-899x/471/5/052029
- Dutkiewicz M, Machado M (2019b) Spectral element method in the analysis of vibrations of overhead transmission line in damping environment, Structural

- Engineering and Mechanics 71(3) 291–303. URL https://doi.org/10.12989/sem.2019.71.3.291
- Dutkiewicz M and Machado MR (2019c) Dynamic response of overhead transmission line in turbulent wind flow with application of the spectral element method, IOP Conference Series: Materials Science and Engineering 471 524.
- El-Borgi PRJDS and Fernandes R (2020) Multiple bandgap formation in a locally resonant linear metamaterial beam: Theory and experiments. *Journal* of Sound and Vibration 488, 115647.
- Friswell M and Mottershead J (1995) Finite Element Model Updating in Structural Dynamics. Dordrecht, The Netherlands: Kluwer Academic Publishers
- Gao N, Wang M and Cheng B (2022) Deep auto-encoder network in predictive design of helmholtz resonator: On-demand prediction of sound absorption peak. Applied Acoustics 191, 108680. https://doi.org/10.1016/j.apacoust.2022.108680.
- Goh H, Kallivokas LF (2019) Inverse metamaterial design for controlling band gaps in scalar wave problems, Wave Motion 88 85–105. https://doi. org/10.1016/j.wavemoti.2019.02.001
- Guo X, Zhang J, Zong S and Zhu S (2023) A fast-response-generation method for single-layer reticulated shells based on implicit parameter model of generative adversarial networks. *Journal of Building Engineering* 72, 106563. https://doi.org/10.1016/j.jobe.2023.106563.
- Han Z, Wei K, Liu YLX, Li J and Chen X (2023) Developing mechanical metamaterials under an adaptable topology optimization design framework. *Acta Mechanica Solida Sinica* 36, 306–316. https://doi.org/10.1007/s10338-023-00379-v.
- Harper ES, Coyle EJ, Vernon JP, Mills MS 2020 Inverse design of broadband highly reflective metasurfaces using neural networks, *Physical Review B* 101 (May). https://doi.org/10.1103/PhysRevB.101.195104.
- He L, Guo H, Jin Y, Zhuang X, Rabczuk T, Li Y, Machine-learning-driven on-demand design of phononic beams, Science China: Physics, Mechanics and Astronomy 65 (2022) 1–12. https://doi.org/10.1007/s11433-021-1787-x.
- He L, Li Y, Torrent D, Zhuang X, Rabczuk T and Jin Y (2023) Machine learning assisted intelligent design of meta structures: A review. *Microstructures* 3. https://doi.org/10.20517/microstructures.2023.29.
- Helton J and Davis F (2003) Latin hypercube sampling and the propagation of uncertainty in analyses of complex systems. *Reliability Engineering & System Safety* 81 (1), 23–69. https://doi.org/10.1016/S0951-8320(03)00058-9.
- Hou J, Lin H, Xu W, Tian Y, Wang Y, Shi X, Deng F and Chen L (2020) Customized inverse design of metamaterial absorber based on target-driven deep learning method. *IEEE Access* 8, 211849–211859. https://doi.org/ 10.1109/ACCESS.2020.3038933.
- Hou Z, Tang T, Shen J, Li C and Li F (2020) Prediction network of metamaterial with split ring resonator based on deep learning. *Nanoscale Research Letters* 15. https://doi.org/10.1186/s11671-020-03319-8.
- Hou Z, Zhang P, Ge M, Li J, Tang T, Shen J and Li C (2021) Metamaterial reverse multiple prediction method based on deep learning. *Nanomaterials* 11. https://doi.org/10.3390/nano11102672.
- Hussein MI, Leamy MJ and Ruzzene M (2014) Dynamics of phononic materials and structures: Historical origins, recent progress, and future outlook. *Applied Mechanics Reviews* **66** (4), 1–38.
- Inampudi S and Mosallaei H (2018) Neural network based design of metagratings. Applied Physics Letters 112 (24). https://doi.org/10.1063/1.5033327.
- Jeffcott HH (1918) The periods of lateral vibration of loaded shafts.—The rational derivation of dunkerley's empirical rule for determining whirling speeds. Proceedings of the Royal Society of London. Series A, Containing Papers of a Mathematical and Physical Character 95 (666), 106–115.
- Jiang P, Wang Z, Li X, Wang XV, Yang B and Zheng J (2023) Energy consumption prediction and optimization of industrial robots based on LSTM. Journal of Manufacturing Systems 70, 137–148. https://doi.org/ 10.1016/j.jmsy.2023.07.009.
- Jiang P, Zheng J, Wang Z, Qin Y and Li X (2025) Industrial robot energy consumption model identification: A coupling model-driven and data-driven paradigm. Expert Systems with Applications 262. https://doi.org/10.1016/j. eswa.2024.125604.
- Jiao AAH and Alavi AH (2022) Artificial intelligence-enabled smart mechanical metamaterials: Advent and future trends. *International Materials Reviews* 66 (6), 365–393. https://doi.org/10.1080/09506608.2020.1815394.
- Jin Y, He L, Wen Z, Mortazavi B, Guo H, Torrent D, Djafari-Rouhani B, Rabczuk T, Zhuang X and Li Y (2022) Intelligent on-demand design of

- phononic metamaterials. Nano 11, 439–460. https://doi.org/10.1515/nanoph-2021-0639
- Jin Y, Zeng S, Wen Z, He L, Li Y and Li Y (2022) Deep-subwavelength lightweight metastructures for low-frequency vibration isolation. *Materials & Design* 215, 110499. https://doi.org/10.1016/j.matdes.2022.
- Jonkman JM, Butterfield S, Musial W, Scott G 2009 Definition of a 5-MW reference wind turbine for offshore system development [electronic resource], National Renewable Energy Laboratory. https://www.nrel.gov/docs/fy09osti/38060.pdf
- Jonkman JM, Musial W 2010 Offshore Code Comparison Collaboration (OC3) for IEA Task 23 Offshore Wind Technology and Deployment [Electronic Resource], National Renewable Energy Laboratory. https://www.nrel.gov/docs/fy11osti/48191.pdf
- Khosravi A, Nahavandi S, Creighton D and Atiya AF (2011) Comprehensive review of neural network-based prediction intervals and new advances. *IEEE Transactions on Neural Networks* 22 (9), 1341–1356. https://doi.org/10.1109/ TNN.2011.2162110.
- Li Y, Chen D, Li X and Wang W (2024) Vibration transmission characteristic prediction and structure inverse design of acoustic metamaterial beams based on deep learning. *JVC/Journal of Vibration and Control* 30, 807–821. https://doi.org/10.1177/10775463231151462.
- Li X, Ning S, Liu Z, Yan Z, Luo C and Zhuang Z (2020) Designing phononic crystal with anticipated band gap through a deep learning based data-driven method. Computer Methods in Applied Mechanics and Engineering 361. https://doi.org/10.1016/j.cma.2019.112737.
- Li X, Zhang S, Jiang P, Deng M, Wang XV, Yin C 2024 Knowledge graph based opc ua information model automatic construction method for heterogeneous devices integration, *Robotics and Computer-Integrated Manufacturing* 88 (AUG). https://doi.org/10.1016/j.rcim.2024.102736.
- Liu L and Hussein MI (2012) Wave motion in periodic flexural beams and characterization of the transition between bragg scattering and local resonance. *Journal of Applied Mechanics, Transactions ASME* 79, 1–17. https://doi. org/10.1115/1.4004592.
- Liu FT, Ting KM, Zhou Z-H 2008 Isolation forest, Eighth IEEE International Conference on Data Mining (2008) 413–422 https://doi.org/10.1109/ ICDM.2008.17.
- Liu C-X and Yu GL (2023) Yu, deep learning for the design of phononic crystals and elastic metamaterials. *Journal of Computational Design and Engineering* 10, 602–614. https://doi.org/10.1093/jcde/qwad013.
- Lu H, Cantero-Chinchilla S, Yang X, Gryllias K and Chronopoulos D (2024)
 Deep learning uncertainty quantification for ultrasonic damage identification in composite structures. *Composite Structures* 338, 118087. https://doi.org/10.1016/j.compstruct.2024.118087.
- Ma W, Cheng F and Liu Y (2018) Deep-learning-enabled on-demand design of chiral metamaterials. ACS Nano 126, 6326–6334. https://doi.org/10.1021/ acsnano.8b03569.
- Machado M, Appert A and Khalij L (2019) Spectral formulated modelling of an electrodynamic shaker. *Mechanics Research Communications* 97, 70–78. https://doi.org/10.1016/j.mechrescom.2019.04.014.
- Machado M and Dutkiewicz M (2024) Wind turbine vibration management: An integrated analysis of existing solutions, products, and open-source developments. *Energy Reports* 11, 3756–3791. https://doi.org/10.1016/j. egyr.2024.03.014.
- Machado MR and Dutkiewicz M (2024) Enhancing broadband vibration suppression of a cable conductor using graded metamaterials. *Journal of the Brazilian Society of Mechanical Sciences and Engineering* 46 (190), 1806–3691. https://doi.org/10.1007/s40430-024-04722-3.
- Machado M and Dutkiewicz M (2025) Enhancing vibration attenuation in offshore wind turbine with multiphysics mechanical metamaterial. *Energy Reports* 13, 1780–1801. https://doi.org/10.1016/j.egyr.2025.01.003.
- Machado M, Dutkiewicz M and Colherinhas G (2024) Metamaterial-based vibration control for offshore wind turbines operating under multiple hazard excitation forces. Renewable Energy 223, 120056. https://doi.org/10.1016/j. renene 2024 120056.
- Mahesh K, Ranjith SK and Mini RS (2021) Inverse design of a helmholtz resonator based low-frequency acoustic absorber using deep neural network. *Journal of Applied Physics* **129**. https://doi.org/10.1063/5.0046582.

- Mahesh K, Ranjith S and Mini R (2024) A deep autoencoder-based approach for the inverse design of an acoustic-absorber. *Engineering with Computers* **40**, 279–300. https://doi.org/10.1007/s00366-023-01789-9.
- **Muhammad OO and Kennedy J** (2022) Inverse design of a topological phononic beam with interface modes. *Journal of Physics D: Applied Physics* **56**. https://doi.org/10.1088/1361-6463/ac9ce8.
- Otaru AJ (2023) Research of the numerical simulation and machine learning backpropagation networks analysis of the sound absorption properties of cellular soundproofing materials. *Results in Engineering* **20** (6). https://doi.org/10.1016/j.rineng.2023.101588.
- Peurifoy J, Shen Y, Jing L, Yang Y, Cano-Renteria F, DeLacy BG, Joanno-poulos JD, Soljačić M and Lalor SK (2018) Nanophotonic particle simulation and inverse design using artificial neural networks. *Science. The Advocate* 4 (6). https://doi.org/10.1126/sciadv.aar4206.
- Pillai P, Pal P, Chacko R, Jain D and Rai B (2021) Leveraging long short-term memory (LSTM)-based neural networks for modeling structure–property relationships of metamaterials from electromagnetic responses. Scientific Reports 11, 18629. https://doi.org/10.1038/s41598-021-97999-6.
- Raju L, Lee K-T, Liu Z, Zhu D, Zhu M, Poutrina E, Urbas A and Cai W (2022) Maximized frequency doubling through the inverse design of nonlinear metamaterials. ACS Nano. https://doi.org/10.1021/acsnano.1c09298.
- Reis FD and Karathanasopoulos N (2022) Inverse metamaterial design combining genetic algorithms with asymptotic homogenization schemes. *International Journal of Solids and Structures* 250, 111702. https://doi.org/10.1016/j.ijsolstr.2022.111702.
- Ren H, Liu S, Qiu B, Guo H and Zhao D (2024) A novel intelligent fault diagnosis method of bearing based on multi-head self-attention convolutional neural network. Artificial Intelligence for Engineering Design, Analysis and Manufacturing 38. https://doi.org/10.1017/S08900604230 00197.
- Shi X, Qiu T, Wang J, Zhao X and Qu S (2020) Metasurface inverse design using machine learning approaches. *Journal of Physics D: Applied Physics* 53 (27). https://doi.org/10.1088/1361-6463/ab8036
- Sinha P and Mukhopadhyay T (2023) Programmable multi-physical mechanics of mechanical metamaterials, materials science and engineering: R. Report 155, 100745. https://doi.org/10.1016/j.mser.2023.100745.
- So S, Badloe T, Noh J, Rho J and Bravo-Abad J (2020) Deep learning enabled inverse design in nanophotonics. Nano 9, 1041–1057. https://doi. org/10.1515/nanoph-2019-0474.
- Soete C, Rademaker M and Hoecke SV (2024) A semi-supervised anomaly detection approach for detecting mechanical failures, artificial intelligence for engineering design. *Analysis and Manufacturing* 38, e16. https://doi. org/10.1017/S0890060424000131.

- Soomro AA, Muhammad aA MMB, Saad MHM, Lashari N, Hussain, Sarwar U and Palli AS (2024) Insights into modern machine learning approaches for bearing fault classification: A systematic literature review. *Results in Engineering* 23. https://doi.org/10.1016/j.rineng.2024.102700.
- Sousa A, Silva C, Machado MR and Dutkiewicz M (2023) Multiclass supervised machine learning algorithms applied to damage and assessment using beam dynamic response. *Journal of Vibration Engineering and Technologies* 11 (6), 2709–2731. https://doi.org/10.1007/s42417-023-01072-7.
- Sridhar A, Kouznetsova V and Geers M (2016) Homogenization of locally resonant acoustic metamaterials towards an emergent enriched continuum. Computational Mechanics 57, 1780–1801. https://doi.org/10.1007/s00466-015-1254-v.
- Sugino LSRM and Erturk CA (2016) On the mechanism of bandgap formation in locally resonant finite elastic metamaterials. *Journal of Applied Physics* **120** (13), 4963648.
- Valipour A, Kargozarfard MH, Rakhshi M, Yaghootian A and Sedighi HM (2022) Metamaterials and their applications: An overview, proceedings of the institution of mechanical engineers. Part L: Journal of Materials: Design and Applications 236 (11), 2171–2210. https://doi.org/10.1177/1464420721995858.
- Wang L, Chan Y-C, Ahmed F, Liu Z, Zhu P and Chen W (2020) Deep Generative Modeling for Mechanistic-Based Learning and Design of Metamaterial Systems ArXiv abs/2006.15274. https://doi.org/10.1016/j.cma.2020.113377
- Wu L and Li Y (2021) Harnessing bulging or sloshing modes to design locally resonant liquid-solid metamaterials. *Journal of Sound and Vibration* 510, 116280. https://doi.org/10.1016/J.JSV.2021.116280.
- Wu RT, Liu TW, Jahanshahi MR and Semperlotti F (2021) Design of onedimensional acoustic metamaterials using machine learning and cell concatenation. Structural and Multidisciplinary Optimization 63, 2399–2423. https://doi.org/10.1007/s00158-020-02819-6.
- Zhang S, Jiang P, Li X, Yin C, Wang XV 2024 A blockchain-empowered secure federated domain generalization framework for machinery fault diagnosis, *Advanced Engineering Informatics* 62 (B) (OCT). https://doi.org/10.1016/j. aei.2024.102756.
- Zhang J, Li Y, Zhao T, Zhang Q, Zuo L and Zhang K (2021) Machine-learning based design of digital materials for elastic wave control. *Extreme Mechanics Letters* 48, 101372. https://doi.org/10.1016/j.eml.2021.101372.
- Zhang C, Xie J, Shanian A, Kibsey M and Zhao YF (2023) A hybrid deep learning approach for the design of 2d low porosity auxetic metamaterials. Engineering Applications of Artificial Intelligence 123, 106413. https://doi. org/10.1016/j.engappai.2023.106413.
- Zhang Q, Zhang K and Hu G (2018) Tunable fluid-solid metamaterials for manipulation of elastic wave propagation in broad frequency range. Applied Physics Letters. https://doi.org/10.1063/1.5023307.